Monthly Notices
of the
ROYAL ASTRONOMICAL SOCIETY

MNRAS **469,** 4763–4787 (2017)
Advance Access publication 2017 May 12

doi:10.1093/mnras/stx1137

A common-envelope wind model for Type Ia supernovae – I. Binary evolution and birth rate

X. Meng[1,2,3★] and Ph. Podsiadlowski[4★]

[1] *Yunnan Observatories, Chinese Academy of Sciences, 650216 Kunming, PR China*
[2] *Key Laboratory for the Structure and Evolution of Celestial Objects, Chinese Academy of Sciences, 650216 Kunming, PR China*
[3] *Center for Astronomical Mega-Science, Chinese Academy of Sciences, 20A Datun Road, Chaoyang District, Beijing 100012, PR China*
[4] *Department of Astronomy, Oxford University, Oxford OX1 3RH, UK*

Accepted 2017 May 9. Received 2017 May 5; in original form 2016 June 28

ABSTRACT

The single-degenerate (SD) model is one of the principal models for the progenitors of Type Ia supernovae (SNe Ia), but some of the predictions in the most widely studied version of the SD model, i.e. the optically thick wind (OTW) model, have not been confirmed by observations. Here, we propose a new version of the SD model in which a common envelope (CE) is assumed to form when the mass-transfer rate between a carbon–oxygen white dwarf (CO WD) and its companion exceeds a critical accretion rate. The WD may gradually increase its mass at the base of the CE. Due to the large nuclear luminosity for stable hydrogen burning, the CE may expand to giant dimensions and will lose mass from the surface of the CE by a CE wind (CEW). Because of the low CE density, the binary system will avoid a fast spiral-in phase and finally re-emerge from the CE phase. Our model may share the virtues of the OTW model but avoid some of its shortcomings. We performed binary stellar evolution calculations for more than 1100 close WD + MS binaries. Compared with the OTW model, the parameter space for SNe Ia from our CEW model extends to more massive companions and less massive WDs. Correspondingly, the Galactic birth rate from the CEW model is higher than that from the OTW model by ∼30 per cent. Finally, we discuss the uncertainties of the CEW model and the differences between our CEW model and the OTW model.

Key words: binaries: close – stars: evolution – supernovae: general – white dwarfs.

1 INTRODUCTION

Being an excellent cosmological distance indicators, Type Ia supernovae (SNe Ia) have been successfully applied to determine cosmological parameters (e.g. Ω and Λ; Riess et al. 1998; Perlmutter et al. 1999). Indeed it has even been proposed that SNe Ia can be used for testing the evolution of the equation of the state of dark energy with time (Howell et al. 2009). SNe Ia also play an important part in understanding the role of galactic chemical evolution as they are believed to be the main producer of iron in their host galaxies (Greggio & Renzini 1983; Matteucci & Greggio 1986). They are also accelerators of cosmic rays and sources of kinetic energy in galaxy evolution processes (Helder et al. 2009; Powell, Slyz & Devriendt 2011).

It is widely accepted that SNe Ia originate from the thermonuclear runaway of a carbon–oxygen white dwarf (CO WD) in a binary system. The CO WD accretes material from its companion, increases mass to its maximum stable mass and then explodes as a thermonuclear runaway. Almost half of the WD mass is converted into radioactive ^{56}Ni during the explosion (Branch 2004), and the amount of ^{56}Ni determines the maximum luminosity of SNe Ia (Arnett 1982). However, the precise nature of the progenitor systems remains unclear (Branch et al. 1995; Hillebrandt & Niemeyer 2000; Leibundgut 2000; Maoz, Mannucci & Nelemans 2014), although the identification of the progenitor has wide-ranging implications in a number of related astrophysical fields (Wang & Han 2012; Meng, Gao & Han 2015). There have been two main competing scenarios for the last four decades for the progenitor systems of SNe Ia, which depend on the nature of the companion star. In the single-degenerate (SD) model, a CO WD grows in mass by accretion from its non-degenerate companion (Whelan & Iben 1973; Nomoto, Thielemann & Yokoi 1984) while, in the double-degenerate (DD) scenario, two WDs merge after losing angular momentum by gravitational-wave radiation (Iben & Tutukov 1984; Webbink 1984). There is some support for both models, but there also are some serious problems, both on the observational as well as the theoretical side (Howell 2011; Maoz et al. 2014). In this paper, we focus on the SD model.

In the standard SD model, the maximum stable mass of a CO WD is close to the Chandrasekhar mass (∼1.378 $M_\odot$, Nomoto et al.

★ E-mail: xiangcunmeng@ynao.ac.cn (XM); podsi@astro.ox.ac.uk (PhP)

© 2017 The Authors
Published by Oxford University Press on behalf of the Royal Astronomical Society

Downloaded from https://academic.oup.com/mnras/article-abstract/469/4/4763/3820926
by Said Business School user
on 16 February 2018

1984). The companion of the WD may be a main-sequence star or a sub-giant star (WD+MS), or a red-giant star (WD+RG) (Yungelson et al. 1995; Li & van den Heuvel 1997;Hachisu et al. 1999a; Hachisu, Kato & Nomoto 1999b; Nomoto et al. 1999; Langer et al. 2000; Han & Podsiadlowski 2004). There is substantial observational support for the SD model: e.g. the detection of circumstellar material (CSM) in the spectrum of SNe Ia is usually taken as strong evidence in favour of the SD model (Patat et al. 2007; Sternberg et al. 2011; Dilday et al. 2012; Maguire et al. 2013). Moreover, supersoft X-ray sources (SSSs, WD + MS or WD + RG systems, van den Heuvel 1992; Di Stefano & Kong 2003) have been proposed to be good candidates as the progenitors of SNe Ia (Hachisu & Kato 2003a,b). Recently, the UV excesses expected from the collision between supernova (SN) ejecta and their companion have been reported, which provides fairly definitive support for the SD model at least in these cases (Kasen 2010; Foley et al. 2012; Brown 2014; Cao et al. 2015, 2016; Graur et al. 2016; Marion et al. 2016). It is therefore quite possible that all SN 2002es-like SNe arise from SD systems (Cao et al. 2016). A direct method for confirming this type of progenitor model is to search for the companion stars of SNe Ia in their remnants. The claimed discovery of a potential companion of Tycho's SN could in principle support the WD + MS model (Ruiz-Lapuente et al. 2004; González-Hernández et al. 2009; Bedin et al. 2014), although there are some strong doubts about this identification (Kerzendorf et al. 2009, 2013). Here, we concentrate on the WD + MS channel, which is likely to be a very important channel for producing SNe Ia in our Galaxy and other late-type galaxies (Han & Podsiadlowski 2004).

Whether a CO WD explodes as an SN Ia in the SD model depends mainly on the mass-transfer rate from its companion. The maximum accretion rate for stable hydrogen burning on a WD surface defines a critical accretion rate, $\dot{M}_{\rm cr}$ (Nomoto 1982; Nomoto et al. 2007). If the mass-transfer rate is larger than $\dot{M}_{\rm cr}$, the WD may expand to become a RG-like object, and then a CE may form which engulfs both the WD and its companion. In the past it had been suggested that the system would then experience a spiral-in phase where the system will ultimately merge and avoid an SN Ia (Nomoto, Nariai & Sugimoto 1979); this is one of the reasons for the low birth rate of SNe Ia from the SD model. To avoid this problem, the optically thick wind (OTW) model was proposed (Hachisu, Kato & Nomoto 1996; Hachisu et al. 1999a,b), in which the accreted hydrogen steadily burns on the surface of the WD at the rate $\dot{M}_{\rm cr}$ while the unprocessed matter is lost from the system as an OTW. Since Hachisu et al. (1996), many studies have been based on the OTW model (Li & van den Heuvel 1997; Han & Podsiadlowski 2004; Chen & Li 2007; Hachisu, Kato & Nomoto 2008; Meng, Chen & Han 2009a; Meng & Yang 2010a; Wang, Li & Han 2010; Chen, Han & Tout 2011; Hachisu et al. 2012). The OTW helps to modify the mass-growth rate of the WD and the mass-transfer rate to avoid the formation of a CE, increasing the birth rate of SNe Ia significantly (Han & Podsiadlowski 2004). The OTW model may also explain the properties of SSSs and recurrent novae (RNe, Hachisu & Kato 2003a,b; Hachisu & Kato 2005, 2006a,b; Hachisu, Kato & Luna 2007).

However, some of the predictions of the model are in conflict with observations. According to the opacity calculations by Iglesias & Rogers (1996), whether the OTW may occur or not is heavily dependent on the Fe abundance. When Z is lower than 0.002, it is found that the opacity is too low to drive a wind, i.e. no OTW occurs (Kobayashi et al. 1998). This implies that there exists a low-metallicity threshold for SNe Ia in contrast to SNe II. However, no such metallicity threshold has been found in galaxy host studies (Prieto et al. 2008; Galbany et al. 2016). For the same reason, SNe Ia are not expected at high redshift ($z > 1.4$, Kobayashi et al. 1998), but recently an SN Ia at $z = 2.26$ was reported (Rodney et al. 2015). Furthermore, some other SNe Ia at high redshift and/or in low-metallicity environments have also been discovered (Frederiksen et al. 2012; Rodney et al. 2012; Jones et al. 2013). The material lost from the binary system in the OTW will shape the CSM around the SN Ia; because of the large wind velocity ($\sim$1000 km s^{-1}), it may create a low-density bubble or wind-blown cavity around the SN Ia. Its modification of the CSM on larger scales could become apparent during the SNR phase. Badenes et al. (2007) tried to search for the signatures of wind-blown cavities in seven young SN Ia remnants that would be expected in the OTW model. Unfortunately, they found that such large cavities are incompatible with the dynamics of the forward shock and the X-ray emission from the shocked ejecta in all seven SN Ia remnants.[1] This result may indicate that the progenitors do not modify their surroundings in a strong way – especially, the absorption features seen in the spectra of SNe Ia suggest small cavities of radius $\sim 10^{17}$ cm (Patat et al. 2007; Blondin et al. 2009; Borkowski, Blondin & Reynolds 2009; Simon et al. 2009; Sternberg et al. 2011; Patnaude et al. 2012). In addition, by modelling two remnants in the Large Magellanic Cloud with strong Fe–L line emission in their interiors, Borkowski, Hendrick & Reynolds (2006) found that the two remnants required a large interior density, which would be expected from a low-velocity pre-explosion wind rather than the fast OTW.

As an alternative, a super-Eddington-wind (SEW) scenario has been suggested which only weakly depends on metallicity (Ma et al. 2013). However, this model also has the wind velocity problem. In addition, whatever in SEW model or in OTW model, there is a fine-tuning problem that how the helium flash and hydrogen burning adjust with each other (e.g. Piersanti et al. 2000; Shen & Bildsten 2007; Woosley & Kasen 2011). This issue is crucial to determine whether or not a CO WD may effectively increase its mass.

If there is no OTW or SEW, the status of the SD model goes back to the situation some 20 yr ago. However, whether the formation of a CE really needs to be avoided, as suggested by Nomoto et al. (1979), has never been properly addressed. In this paper, we constructed a new SD model in which no OTW occurs but a CE forms around the binary systems when the mass-transfer rate exceeds the critical accretion rate. As we will show, a CE does not generally lead to the merger of the binary system as the density in the CE is usually quite low, resulting in a long spiral-in time-scale. Indeed the existence of a temporary CE has many attractive features: the WD will naturally grow at the stable nuclear burning rate, both for H and He shell burning phases (similar to the situation in thermally pulsing asymptotic giant branch [TPAGB] stars), avoiding some of the fine-tuning in the classical SD model. While the CE acts as a mass reservoir, the wind from an extended CE envelope will naturally produce the low velocities in the circumstellar medium (CSM) as inferred for some SNe Ia (Badenes et al. 2007; Patat et al. 2007). As the system will have the appearance of a TPAGB star in the main WD accretion phase, no X-rays are expected, alleviating the existing X-ray constraints on the SD model (Di Stefano 2010;

[1] We notice that Williams (2011) reported results from a multiwavelength analysis of the Galactic SN remnant RCW 86 and found that the observed characteristics of RCW 86 may be reproduced by an off-centre SN explosion in a low-density cavity carved out by the progenitor system. However, the remnant has usually been considered a core-collapse SN (e.g. Ghavamian et al. 2001) although this is still being debated (Broersen et al. 2014).

Downloaded from https://academic.oup.com/mnras/article-abstract/469/4/4763/3820926
by Said Business School user
on 16 February 2018

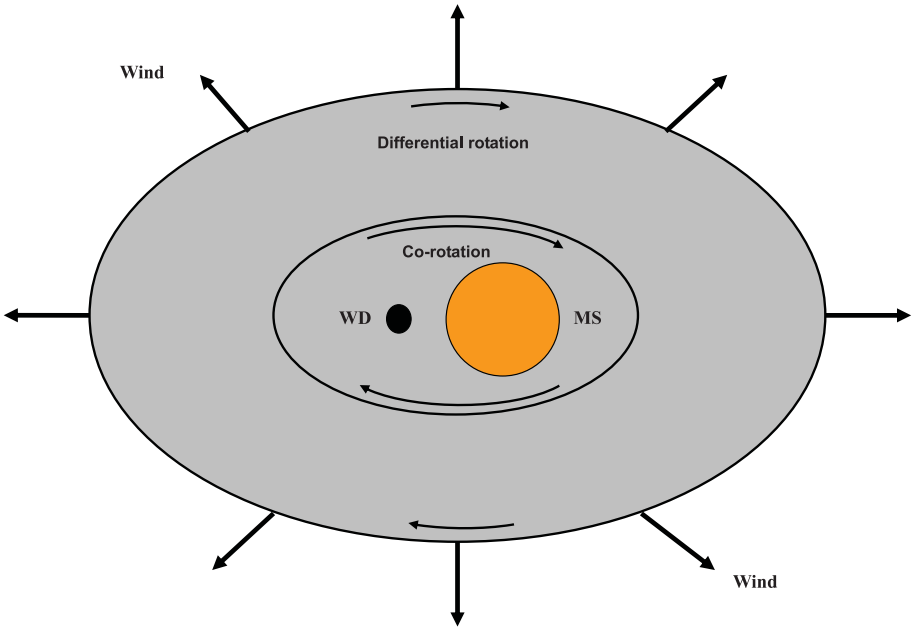

Figure 1. Schematic diagram illustrating the common envelope (CE)-wind model. The mass-transfer rate from the Roche lobe filling companion exceeds the critical accretion rate at which the WD can accrete. This leads to the formation of a CE. The inner region of the CE corotates with the binary, while the outer region rotates differentially. Mass is lost from the surface of the CE, powered in part by the luminosity emitted from the accreting WD and in part by the frictional energy generated in the differentially rotating region.

Gilfanov & Bogdán 2010). In many cases, some H-rich CE material is still left at the time of the explosion. While, in most cases, this will not be directly detectible, it may explain the high-velocity Ca features observed in many SNe Ia which seem to require the existence of some H (Mazzali et al. 2005a,b).

In this paper, we will comprehensibly study this new framework for the SD scenario specifically for the WD + MS channel and systematically determine the parameter space for potential SN Ia progenitors. The results can be applied to study the statistical properties of SNe Ia using a binary population synthesis (BPS) approach and may be helpful in searches for potential progenitor systems of SNe Ia. In Section 2, we describe the detailed numerical method for the binary evolution calculations and the model grid we have calculated. The results of these calculations are presented in Section 3. Our BPS is presented in Section 4, and the BPS results are shown in Section 5. We briefly discuss our results in Section 6. Finally, we summarize the main results in Section 7, where we also discuss the future work required to develop the model further.

2 THE COMMON-ENVELOPE WIND MODEL FOR SNE IA

2.1 Physics input

To calculate the binary evolution of WD+MS systems in detail, we adopt the stellar evolution code developed by Eggleton (1971, 1972, 1973). During the last four decades, the code has been updated repeatedly with the latest input physics (Han, Podsiadlowski & Eggleton 1994; Pols et al. 1995, 1998). For example, Roche lobe overflow (RLOF) is treated as a modification of one boundary condition to ensure that the companion overfills its Roche lobe but never much overfills its Roche lobe for the steady RLOF (Han, Tout & Eggleton 2000). The ratio of mixing length to local pressure scaleheight, $\alpha = l/H_{\rm p}$, is set to be 2.0, and the convective overshooting parameter, $\delta_{\rm OV}$, to be 0.12 (Pols et al. 1997; Schröder, Pols & Eggleton 1997), which roughly equals to an overshooting length of $0.25H_{\rm P}$. Solar metallicity, i.e. $Z = 0.02$, is adopted in this paper. The opacity tables have been compiled by Chen & Tout (2007) from Iglesias & Rogers (1996) and Alexander & Ferguson (1994).

2.2 Model

In the WD + MS channel,[2] the companion fills its Roche lobe on the main sequence or in the Hertzsprung gap (HG) and transfers material on to the WD. If the mass-transfer rate, $|\dot{M}_2|$, exceeds the critical value, $\dot{M}_{\rm cr}$, the WD will become an RG-like object and fill and ultimately overfill its Roche lobe. A CE then forms. Hereafter, we shall refer to our model as the CE wind (CEW) model to distinguish it from the original OTW model (Fig. 1 provides a schematic cartoon of the CEW model).[3] For the CE structure, our model is similar to that in Meyer & Meyer-Hofmeister (1979). In the model of Meyer & Meyer-Hofmeister (1979), the CE is divided into two regions, i.e. a rigid rotating inner region and a differentially rotating outer region with a simply assumed sharp boundary at distance $s \simeq a$, where a is the binary separation. The inner region corotates with the binary, while the angular frequency of the outer region drops

[2] We also plan to apply the CEW model to the WD + RG channel in the future, once the model has been developed sufficiently, as the WD + RG channel may be essential for producing SNe Ia in old populations. See Section 6.1 where we discuss some of the key uncertainties in our model.

[3] Note that our model differs significantly from the core-degenerate model, in which the CE forms on a dynamical time-scale and the newly formed binary in the CE consists of the WD and the hot core of an AGB star (Soker 2013; Ilkov & Soker 2012, 2013), while for our CEW model, the CE is maintained on a thermal time-scale, and the binary embedded in the CE consists of a WD + MS system.

Downloaded from https://academic.oup.com/mnras/article-abstract/469/4/4763/3820926
by Said Business School user
on 16 February 2018

off as a power law, which means that at the boundary between the inner and outer regions, the angular frequency of the CE equals the orbital angular frequency of the inner binary system. Here, we also assume, as in Meyer & Meyer-Hofmeister (1979), that the inner region of the CE corotates with the binary while the outer region rotates differentially. The differentially rotating outer envelope continually extracts the orbital angular momentum from the inner binary to the slowly rotating outer part at a rate

$$\dot{I} = -\alpha\eta a^3\Omega, \tag{1}$$

where a is the binary separation, Ω is the Keplerian orbital angular frequency of the WD + MS binary,

$$\Omega^2 = \frac{G(M_1+M_2)}{a^3}, \tag{2}$$

η is the effective turbulent viscosity,

$$\eta = \rho l v_c/2 \tag{3}$$

(ρ is the CE density, v_c the convective velocity, l the mixing length) taken at the boundary of the corotating inner region, i.e. $s \simeq a$ and α is a coefficient of order one. Then, the friction between the inner and the outer regions of the CE leads to a decrease of the orbital angular momentum

$$I = \frac{M_1M_2}{M_1+M_2}a^2\Omega, \tag{4}$$

and the energy released by the shrinking binary orbit is

$$L_f = \frac{d}{dt}\left(\frac{GM_1M_2}{2a}\right) = \alpha\eta G(M_1+M_2). \tag{5}$$

Actually, almost all of the potential energy released is dissipated as frictional heat and added to the nuclear energy to expand the CE, where α represents the efficiency of transferring the orbital angular momentum of the inner binary system to the angular momentum of the outer CE (see equation 1). Here, guided by the results of Meyer & Meyer-Hofmeister (1979), we[4] simply set $\alpha = 10$, $l = 0.1\,a$ and $v_c = 0.26\sqrt{GM_\odot/a}$. We also treat the CE as spherical and ρ in equation (3) is set to be the average density of the CE

$$\overline{\rho} = \frac{M_{CE}}{(4/3)\pi R_{CE}^3}, \tag{6}$$

where M_{CE} is the CE mass, which is derived from

$$\dot{M}_{CE} = |\dot{M}_2| - \dot{M}_{WD} - \dot{M}_{wind}. \tag{7}$$

$\dot{M}_{wind}$ is the mass-loss rate from the CE surface due to a wind, which is obtained by modifying the Reimer's wind formula (Reimers 1975):

$$\dot{M}_{wind} = 1\times10^{-13}\frac{(L_{tot}/L_\odot)(R_{CE}/R_\odot)}{(M_1+M_2+M_{CE})/M_\odot}\,M_\odot\,yr^{-1}, \tag{8}$$

where $L_{tot} = L_{nuc} + L_2 + L_f$. Here, L_2 is the secondary luminosity and L_{nuc} is the nuclear energy for stable hydrogen burning

$$L_{nuc} = 0.007X\dot{M}_{cr}c^2, \tag{9}$$

where X is the hydrogen mass fraction.

Assuming that the system can be modelled as a red-giant star, the effective temperature, radius and mass of system approximately follow the relation

$$\frac{T_{eff}}{T_{eff,\odot}} = \left(\frac{R_{CE}}{R_\odot}\right)^{-0.1}\left(\frac{M_{WD}+M_2+M_{CE}}{M_\odot}\right)^{0.1}, \tag{10}$$

where $T_{eff,\odot}$ and $R_\odot$ are the solar effective temperature and radius, respectively (Wu, Li & Hekker 2014). The effective temperature of the CE should be between 2500 and 3200 K (Schröder & Cuntz 2007). For simplicity, we set the effective temperature of the CE to 3000 K; then the radius of the CE[5] can be obtained from equation (10). Based on equations (7), (8) and (10), we may calculate the CE mass as

$$M_{CE,i+1} = M_{CE,i} + \dot{M}_{CE,i}\cdot\Delta t, \tag{11}$$

where Δt is the time step in the binary evolution calculation, and $M_{CE,0} = 0$ before the mass-transfer rate exceeds the critical accretion rate. (See the Appendix for details on how the CE mass is calculated in practice.)

$\dot{M}_{WD}$ in equation (7) is the mass-growth rate of the WD, which depends on the critical accretion rate (Hachisu et al. 1999a)

$$\dot{M}_{cr} = 5.3\times10^{-7}\frac{(1.7-X)}{X}(M_{WD}-0.4)\,M_\odot\,yr^{-1}, \tag{12}$$

where X is the hydrogen mass fraction and M_{WD} the mass of the accreting WD (in $M_\odot$). If the CE exists, the structure of the WD is similar to a TPAGB star, and we therefore set $\dot{M}_{WD} = \dot{M}_{cr}$, where hydrogen is stably burning into helium, and helium flash and hydrogen-burning phases adjust themselves just as they do in a TPAGB star. When the mass-loss rate from equation (8) is very high, a CE cannot be maintained even if the mass-transfer rate is higher than the critical accretion rate. In this case, we set $\dot{M}_{wind} = |\dot{M}_2| - \dot{M}_{WD} = |\dot{M}_2| - \dot{M}_{cr}$. In the OTW model, when $|\dot{M}_2| > \dot{M}_{cr}$, $\dot{M}_{WD} = \eta_{He}\dot{M}_{cr}$, where η_{He} is the mass accumulation efficiency for helium flashes. Actually, even if a WD accretes hydrogen-rich material at the rate of $\dot{M}_{cr}$, helium burning is always unstable, i.e. helium flashes occur, leading to $\eta_{He} < 1$ even though $|\dot{M}_2| > \dot{M}_{cr}$ (Kato & Hachisu 2004). In Section 6.2, we will discuss the effect of η_{He} on the results of our model. So, in our CEW model, the mass-growth rate of the WD during the phase when $|\dot{M}_2| > \dot{M}_{cr}$ is higher than that in the classical OTW model.

The total luminosity may exceed the Eddington luminosity of the system,

$$L_{Edd} = \frac{4\pi G\,(M_{WD}+M_2+M_{CE})\,c}{\kappa_T} \simeq 3.3\times10^4\frac{M_{WD}+M_2+M_{CE}}{M_\odot}\,L_\odot, \tag{13}$$

where c is the speed of light and κ_T is the Thomson opacity. When the total luminosity exceeds the Eddington luminosity, the common envelope will expand and lose its material at a high mass-loss rate.

[4] At present, the CE model is still very simple and many parameters are quite uncertain, especially the frictional density. Here, the chosen values for some of the parameters are just set for guidance to mainly set the scale of the frictional density. Generally, $\eta \propto l$; the mixing length will be much less than a but a significant fraction of it and we, somewhat arbitrarily, set $l = 0.1\,a$. Our choice of values for α and l results in $\alpha\eta \propto a$, which is of the same order as estimated by Meyer & Meyer-Hofmeister (1979) ($\alpha = 6\pi$ in Meyer & Meyer-Hofmeister 1979). Therefore, the uncertainties of α and η are transferred into an uncertainty in the frictional density. We will discuss the influence of the frictional density on our model in detail in Section 6.1.

[5] The radius of the CE in the CEW model may be larger than 500 $R_\odot$; then the wind velocity from the CE surface is very likely to be lower than 50 km s^{-1}, consistent with the observations of the variable Na absorption lines in the spectrum of some SNe Ia (Patat et al. 2007; Simon et al. 2009).

Downloaded from https://academic.oup.com/mnras/article-abstract/469/4/4763/3820926
by Said Business School user
on 16 February 2018

Both of these effects decrease the CE density and hence the frictional density between the binary system and the CE. As a consequence, the frictional luminosity will decrease until $L_{\rm tot} = L_{\rm Edd}$. However, the mass-loss rate and/or the expanding speed of the CE are quite uncertain, and it is difficult to obtain the frictional density ($L_{\rm f}$) directly. Since the CE may self-regulate to maintain $L_{\rm tot} \simeq L_{\rm Edd}$ by expanding or losing material at a high mass-loss rate, we set the frictional luminosity to be $L_{\rm f} = L_{\rm Edd} - L_{\rm nuc} - L_2$ if the total luminosity exceeds the Eddington luminosity of the system, and

$$\frac{\dot{I}}{I} = -\frac{L_{\rm f} a}{G M_{\rm WD} M_2}, \tag{14}$$

and

$$\dot{M}_{\rm wind} = 1 \times 10^{-13} \frac{(L_{\rm Edd}/{\rm L}_\odot)(R_{\rm CE}/{\rm R}_\odot)}{(M_1 + M_2 + M_{\rm CE})/{\rm M}_\odot} \, {\rm M}_\odot \, {\rm yr}^{-1}. \tag{15}$$

If the CE does not exist, our treatment on the WD mass growth is similar to that in Han & Podsiadlowski (2004) and Meng et al. (2009a), i.e. our CEW model reduces to the OTW model. (1) When $|\dot{M}_2|$ is higher than $\frac{1}{2}\dot{M}_{\rm cr}$, hydrogen shell burning is steady and no mass is lost from the system. The systems at this phase may show the properties of SSSs. (2) When $|\dot{M}_2|$ is lower than $\frac{1}{2}\dot{M}_{\rm cr}$ but higher than $\frac{1}{8}\dot{M}_{\rm cr}$, a very weak shell flash is triggered but no mass is lost from the system. The systems at this phase may show the properties of RNe. (3) When $|\dot{M}_2|$ is lower than $\frac{1}{8}\dot{M}_{\rm cr}$, the hydrogen-shell flash is too strong to accumulate material on the surface of the CO WD. Then, $\dot{M}_{\rm WD}$ is determined by

$$\dot{M}_{\rm WD} = \eta_{\rm He}\eta_{\rm H}|\dot{M}_2|, \tag{16}$$

where $\eta_{\rm H}$ and $\eta_{\rm He}$ are the mass accumulation efficiencies for hydrogen burning and helium flashes, respectively,

$$\eta_{\rm H} = \begin{cases} 1, & \dot{M}_{\rm cr} \geq |\dot{M}_2| \geq \frac{1}{8}\dot{M}_{\rm cr}, \\ 0, & |\dot{M}_2| < \frac{1}{8}\dot{M}_{\rm cr}; \end{cases} \tag{17}$$

$\eta_{\rm He}$ is taken from Kato & Hachisu (2004), and the treatment of $\eta_{\rm He}$ is the same to that in Meng et al. (2009a). We will discuss the effects of $\eta_{\rm He}$ on the final results in Section 6.2.

The model described above is still very simplistic and contains several rather uncertain variables, such as the CE density that has a major effect on the evolution of the system. We will discuss the effects of these uncertainties in some detail in Section 6.1.

We incorporated our model into the Eggleton stellar evolution code and followed the evolution of the mass donor and the mass growth of the accreting CO WD. We calculated more than 1100 WD+MS binary sequences with different initial WD masses, initial secondary masses and initial orbital periods, obtaining a rather dense grid of models. The initial masses of donor stars, $M_2^{\rm i}$, range from 1.8 to 4.1 $\rm M_\odot$; the initial masses of the CO WDs, $M_{\rm WD}^{\rm i}$, from 0.65 to 1.20 $\rm M_\odot$; the initial orbital periods of binary systems, $P^{\rm i}$, from the minimum value, where a zero-age main-sequence (ZAMS) star just fills its Roche lobe, to ∼15 d, at which the companion star fills its Roche lobe at the end of the HG. In this paper, we assume that an SN Ia occurs if the mass of the CO WD reaches 1.378 $\rm M_\odot$, i.e. a value close to the Chandrasekhar mass limit for non-rotating WDs (Nomoto et al. 1984).[6]

[6] As rotating WDs may explode at a higher mass than $M_{\rm WD} = 1.378\,{\rm M}_\odot$, we continue our calculations beyond this mass, assuming the same WD growth pattern as for $M_{\rm WD} < 1.378\,{\rm M}_\odot$ until $M_{\rm WD} = 1.45\,{\rm M}_\odot$ or until the mass-transfer rate falls beyond a threshold value.

3 BINARY EVOLUTION RESULTS

3.1 Binary evolution sequences for three examples in the CEW model

For a WD + MS system, if the mass-transfer rate, $|\dot{M}_2|$, exceeds the critical value, $\dot{M}_{\rm cr}$, the WD will become an RG-like object and fill and ultimately overfill its Roche lobe. Then, a CE forms. The binary system will spiral in because of the frictional drag caused by the CE. If the spiral-in process is very fast, the system could merge and then no SN Ia occurs. Whether the binary system avoids a merger fate in the CE phase is determined by the competition between the mass-transfer time-scale and the merger time-scale, i.e. the system may re-emerge from the CE phase if the merger time-scale is longer than the mass-transfer time-scale; otherwise a merger is unavoidable. In the following, we show some typical binary evolution sequences in our CEW model. The evolution of the binary system in the CEW model is similar to that of the OTW model presented in Han & Podsiadlowski (2004), but some of the details can be quite different. In Figs 2 and 3, we present an example to compare the differences between the CEW model and the OTW model. Fig. 2 shows the evolution of the key binary parameters, including the merger time-scale, as well as the evolutionary tracks of the donor stars in the Hertzsprung–Russell (HR) diagram, and the evolution of the orbital period. In this example, the initial system has donor and WD masses of $M_2^{\rm i} = 2.2\,{\rm M}_\odot$ and $M_{\rm WD}^{\rm i} = 0.8\,{\rm M}_\odot$, respectively, and an initial orbital period of $\log(P^{\rm i}/{\rm d}) = 0.40$. The donor star fills its Roche lobe in the HG, i.e. the system experiences early Case B RLOF. The mass-transfer rate exceeds $\dot{M}_{\rm cr}$ soon after the onset of RLOF, leading to the formation of a CE, where part of the CE material is lost from the surface of the CE. The mass of the CE is always lower than $7 \times 10^{-4}\,{\rm M}_\odot$. After about 1.1×10^6 yr, the mass-transfer rate has decreased below the critical accretion rate, and the CE disappears. During the CEW phase, the CEW has a similar effect as the OTW in the sense of balancing the mass-transfer rate and the accretion rate of the WD, except that the wind velocity from the CE surface is much lower than in the OTW. When the mass-transfer rate drops below $\dot{M}_{\rm cr}$, but is still higher than $\frac{1}{2}\dot{M}_{\rm cr}$, mass loss stops; as hydrogen shell burning is still stable, the WD continues to gradually increase its mass. When the WD mass reaches $M_{\rm WD}^{\rm SN} = 1.378\,{\rm M}_\odot$, the WD is assumed to explode as a SN Ia. At this point, the mass of the donor is $M_2^{\rm SN} = 0.9682\,{\rm M}_\odot$, and the orbital period is $\log(P^{\rm SN}/{\rm d}) = 0.1076$. Note that in panel (3) of Fig. 2, there is a jump in the mass-loss rate just after 1.1×10^6 yr. This jump is caused by the different helium accumulation efficiencies for different WD masses in the model of Kato & Hachisu (2004), which may also lead to a very small jump in $\dot{M}_{\rm WD}$ although it is insignificant in panel (3) of Figs 2 and 3 (see the treatment of $\eta_{\rm He}$ in Meng et al. 2009a and the small jump of $\dot{M}_{\rm WD}$ in fig. 1 of Meng & Yang 2010a). Panel (4) of Fig. 2 shows that the frictional luminosity between the binary system and the CE is very low during the CE phase; as a consequence, the merger time-scale due to the friction in the CE is much longer than the mass-transfer time-scale, i.e. the CE does not strongly affect the evolution of the binary parameters, and the system avoids a merger in the CE phase.

The evolution of the binary system in the OTW model (Fig. 3) is quite similar to that of the CEW model (Fig. 2), i.e. RLOF begins in the HG and the WD explodes during a phase where hydrogen shell burning is stable. When the WD mass reaches $M_{\rm WD}^{\rm SN} = 1.378\,{\rm M}_\odot$, the parameters of the binary system are $(M_2^{\rm SN}, \log P^{\rm SN}) = (0.8578, 0.1653)$. In Fig. 3, the mass-loss rate from the system is the difference between the mass-transfer rate and the mass-growth rate of the WD. The steps in the mass-loss

Downloaded from https://academic.oup.com/mnras/article-abstract/469/4/4763/3820926
by Said Business School user
on 16 February 2018

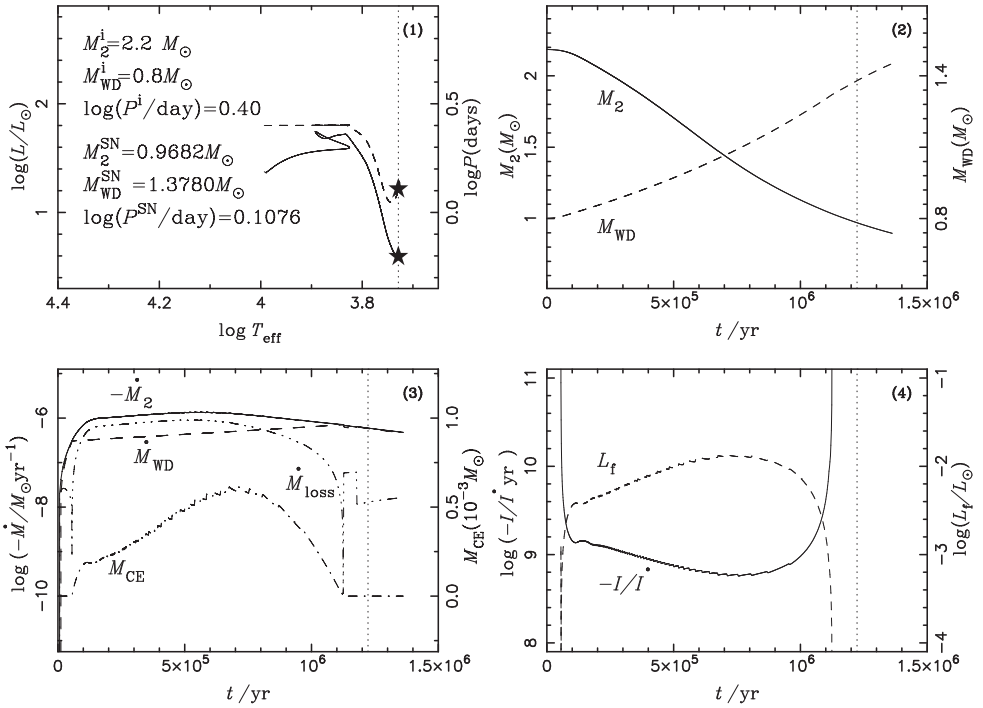

Figure 2. An example of the evolution of a binary in the CEW model. The evolution of various parameters are shown, including the CO WD mass, $M_{\rm WD}$, the secondary mass, M_2, the mass-transfer rate, $\dot{M}_2$, the mass-growth rate of the CO WD, $\dot{M}_{\rm WD}$, the mass of the CE, $M_{\rm CE}$, the mass-loss rate from the system, $\dot{M}_{\rm loss}$, the frictional luminosity, $L_{\rm f}$, and the merger time-scale for the binary system, $I/\dot{I}$, as labelled in each panel. The evolutionary tracks of the donor stars are shown as solid curves and the evolution of the orbital periods is shown as dashed curves in panel (1). Dotted vertical lines in all panels and asterisks in panel (1) indicate the position where the WD is expected to explode as an SN Ia. The initial binary parameters and the binary parameters at the time of the SN Ia explosion are also given in panel (1).

rate in panel (3) of Fig. 3 are caused by the assumptions about the different helium accumulation efficiencies for different WD masses.

However, many details are different in Figs 2 and 3. For example, compared to the final state of the system in Figs 2 and 3, a slightly more massive final secondary and a shorter orbital period are found in the CEW model. The differences are mainly caused by the different treatment of the mass-growth rate of the CO WD when $|\dot{M}_2|$ is larger than $\dot{M}_{\rm cr}$. At this stage, the mass-growth rate of the CO WD for the CEW model is always higher than in the OTW model, i.e. the WD may increase its mass more efficiently in the CEW model than in the OTW model when $|\dot{M}_2|$ exceeds $\dot{M}_{\rm cr}$. Another reason contributing to the differences is the friction between the CE and the binary system which extracts orbital angular momentum from the binary system, leading to a slightly shorter orbital period. For these reasons, the WD in the CEW model also explodes earlier than in the OTW model by about $\sim 2 \times 10^5$ yr.

Actually, all the WD + MS systems that can explode as SNe Ia in the OTW model will also explode in the CEW model, while some that cannot explode in the OTW model do so in the CEW model. Figs 4 and 5 show such an example. In this example, both the WD and the donor are relatively massive. The initial binary parameters in this case are $M_{\rm WD}^{\rm i} = 1.1\,{\rm M}_\odot$, $M_2^{\rm i} = 3.3\,{\rm M}\odot$ and $\log(P^{\rm i}/{\rm d}) = 0.60$. For both models, the donor star fills its Roche lobe in the HG. The mass-transfer rate exceeds $\dot{M}_{\rm cr}$ soon after the onset of RLOF which results in the formation of the CE (or the onset of the OTW). The WD then gradually grows its mass, but the final fate in the two models is quite different, i.e. the WD mass in the CEW model increases to $M_{\rm WD}^{\rm SN} = 1.378\,{\rm M}_\odot$ when $M_{\rm CE} = 0.1559\,{\rm M}_\odot$, while the WD does not reach this mass in the OTW model before the mass-transfer rate drops below $\frac{1}{8}\dot{M}_{\rm cr}$, below which novae are assumed to prevent any further mass accumulation on the WD. The different fate between the two models is again caused by the different treatment of the mass-growth rate of the CO WD when $|\dot{M}_2| > \dot{M}_{\rm cr}$. In addition, because of the effect of the CE on the orbital period, the moment at which the mass-transfer rate drops below $\dot{M}_{\rm cr}$ is slightly delayed, which may also be responsible for the different fate between the CEW model and the OTW model. Moreover, due to the existence of the CE, the mass-growth rate of the WD may still maintain a high value even when $|\dot{M}_2| < \dot{M}_{\rm WD}$.

As Figs 2 and 4 show, the CE mass is much larger in the simulations in Fig. 4 than in Fig. 2. At the moment when $M_{\rm WD}^{\rm SN} = 1.378\,{\rm M}_\odot$, the CE is still as massive as $0.1559\,{\rm M}_\odot$ (see panel 3 of Fig. 4). So, the mass-growth rate of the CO WD can maintain a high value even when $|\dot{M}_2|$ is lower than $\dot{M}_{\rm WD}$. Furthermore, the frictional luminosity in Fig. 4 is also much larger than that in Fig. 2 because of the more massive CE. Even though the frictional merger time-scale in Fig. 4 is shorter than that in Fig. 2, it is still longer than the mass-transfer time-scale, i.e. the effect of the CE on the binary evolution may still be small even for a CE of $\sim 0.7\,{\rm M}_\odot$. Actually, if the frictional luminosity is lower than several 10^2–$10^3\,{\rm L}_\odot$, the binary system may survive from the CE phase irrespective of the CE mass.

Fig. 6 illustrates a more extreme case where both the donor and the WD are relatively massive, but the initial orbital period is shorter than that in Fig. 4. The initial binary parameters in this case are $M_{\rm WD}^{\rm i} = 1.1\,{\rm M}_\odot$, $M_2^{\rm i} = 3.1\,{\rm M}_\odot$ and $\log(P^{\rm i}/{\rm d}) = -0.10$. For this short initial orbital period, the donor star starts to fill its Roche lobe on the MS. In the first $\sim 4 \times 10^5$ yr, the donor loses about $0.5\,{\rm M}_\odot$

Downloaded from https://academic.oup.com/mnras/article-abstract/469/4/4763/3820926
by Said Business School user
on 16 February 2018

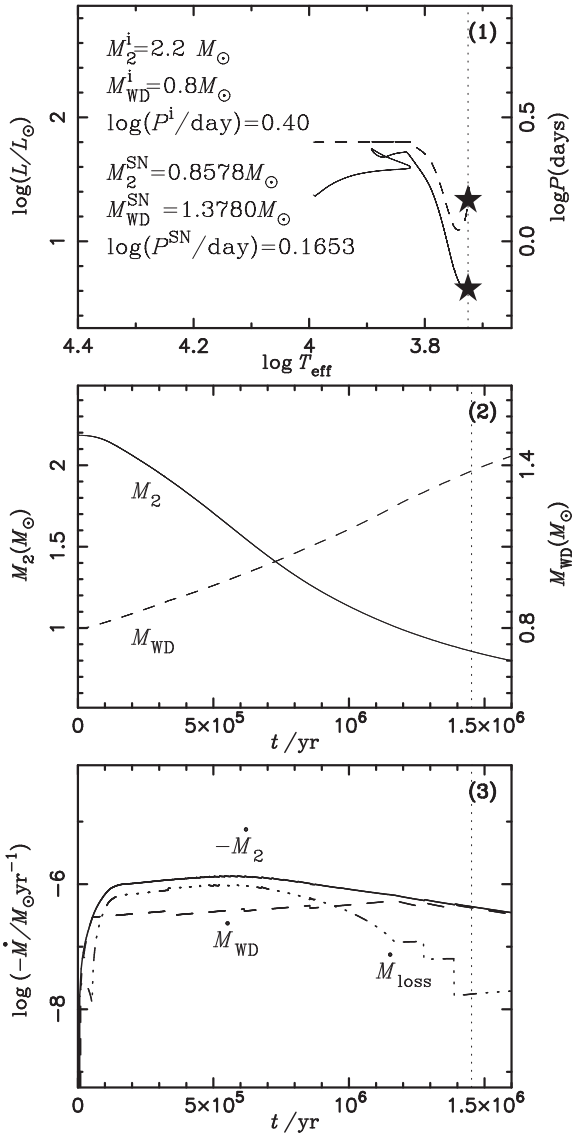

Figure 3. An example of a binary evolution sequence in the OTW model. The evolution of various parameters are shown here, including the CO WD mass, $M_{\rm WD}$, the secondary mass, M_2, the mass-transfer rate, $\dot{M}_2$, the mass-loss rate from the system, $\dot{M}_{\rm loss}$, and the mass-growth rate of the CO WD, $\dot{M}_{\rm WD}$ as labelled in each panel. The evolutionary tracks of the donor stars are shown as solid curves, and the evolution of the orbital period is shown as a dashed curve in panel (1). Dotted vertical lines in all panels and asterisks in panel (1) indicate the position where the WD is expected to explode as a SN Ia. The initial binary parameters and the binary parameters at the time of the SN Ia explosion are also given in panel (1).

after the onset of RLOF. At this stage, mass transfer almost becomes dynamically unstable, and hence the mass-transfer rate increases sharply, as does the CE mass. Within the following $\sim 5 \times 10^4$ yr, the companion loses about 1 $M_\odot$. The mass-transfer rate drops only after the mass ratio has been reversed. The binary parameters at the explosion are $(M_2^{\rm SN}, \log P^{\rm SN}) = (1.1941, -0.4429)$. For an even larger initial donor mass, e.g. $M_2^{\rm i} = 3.2\,M_\odot$, our calculations show that mass transfer becomes unstable, and such systems may experience a delayed dynamical instability (Hjellming & Webbink 1987), i.e. the system may merge completely (but also see Han & Podsiadlowski 2006). Notice that the oscillations in some curves in Fig. 6 are numerical artefacts caused by the high mass-loss rate of the donor for this binary system.

3.2 Final outcomes of the binary evolution calculations

To clearly show the difference between our results and previous ones in literatures, we show the final outcomes of all the binary evolution calculations in an initial orbital period – secondary mass (log $P^{\rm i}$, $M_2^{\rm i}$) plane (Fig. 7). As the figure shows, CO WDs may reach a mass of 1.378 $M_\odot$ while the system is still in the CE phase (filled squares) or after the CE evolution has ended, where they can be either in stable (filled circles) or weakly unstable (filled triangles) hydrogen-burning phases. Systems re-emerging from the CE phase may show the properties of SSSs if hydrogen burning on the WD is stable or those of RNe for weakly unstable hydrogen burning. All these systems are probably progenitors of SNe Ia. Because of dynamically unstable mass transfer or strong hydrogen shell flashes, many CO WDs do not increase their masses to 1.378 $M_\odot$. As shown in Figs 4 and 5, in comparison to the OTW model, the longer time-scale for the CEW phase and the higher mass-growth rate during this phase result in a larger increase of the CO WD mass in this phase. Consequently the time-scale from the end of the CEW to the explosion (where the systems may appear as SSSs or RNe) is shorter, or the CO WD, which would not increase to 1.378 $M_\odot$ in the OTW phase, may reach 1.378 $M_\odot$ during the CEW phase (the system then will not appear as an SSS or RN system). This means that a given system is less likely to be in the SSS/RN phase at the SN explosion in the CEW model (Meng et al. 2009a; Meng, Yang & Geng 2009c). Based on the supersoft X-ray flux in elliptical galaxies, Gilfanov & Bogdán (2010) concluded that no more than 5 per cent of SNe Ia in early-type galaxies can be produced by mass-accreting white dwarfs from the SD scenario. According to the OTW model, Meng & Yang (2011b) found that the mean relative duration of the SSS phase for an accreting WD is about 5 per cent. However, based on the small number of SSSs observed in some galaxies such as M31, Maoz et al. (2014) argued that no more than 1 per cent of the WD's growth time is spent in the SSS phase. This is an order of magnitude less than that found by Meng & Yang (2011b). The results here should help to resolve the conflict between Maoz et al. (2014) and Meng & Yang (2011b) since the CE phase in the CEW model lasts longer than the OTW phase. Moreover, even if the binary system were in an SSS phase, the supersoft X-ray flux would also be strongly reduced by the CSM that forms because of the CEW or the OTW, but the CSM from our CEW model would be more efficient in suppressing the supersoft X-ray flux because of the relatively high CSM density due to the much lower wind velocity (Nielsen et al. 2013; Wheeler & Pooley 2013).

In Fig. 7 we present contours of the initial parameters leading to SNe Ia for different WD masses, indicating the final state of the system, while Fig. 8 combines the contours in one summary plot. The left boundaries of the contours are determined by the radii of ZAMS stars, i.e. correspond to systems that start RLOF on the ZAMS; systems beyond the right boundaries experience dynamically unstable mass transfer at the base of the red-giant branch (RGB). The upper boundaries are determined by systems that experience a delayed dynamical instability. For the systems above the lower boundaries, the mass-transfer rate is larger than $\frac{1}{8}\dot{M}_{\rm cr}$, which prevents the occurrence of strong hydrogen shell flashes, while, at the same time, the secondaries can provide enough material to feed the growth of the CO WDs to allow it to reach 1.378 $M_\odot$. The figure shows that the initial WD mass significantly affects the upper boundary but not the lower boundary. The upper boundary

Downloaded from https://academic.oup.com/mnras/article-abstract/469/4/4763/3820926
by Said Business School user
on 16 February 2018

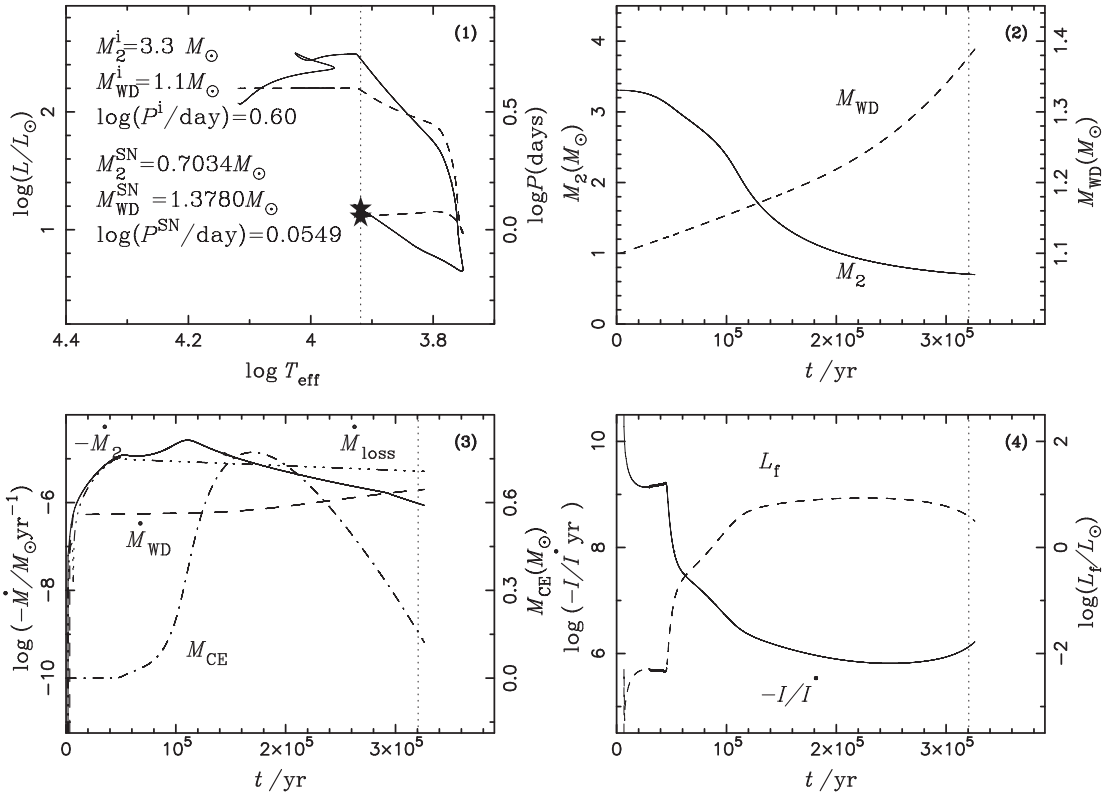

Figure 4. Similar to Fig. 2 for different initial binary parameters.

moves to lower masses as the initial WD mass decreases, causing a shrinking of the initial parameter space that leads to SNe Ia with a decrease of the WD mass; at $M_{\rm WD}^{\rm i} = 0.65\,{\rm M}_\odot$ the contour collapses to a point.

3.3 Comparison with the OTW model

Fig. 7 also shows the contours of initial parameters leading to SNe Ia from the OTW model for comparing the two models. The shapes of the contours are quite similar to each other, except that the upper boundary of the CEW model is higher than that in the OTW model and that the maximum initial orbital period for the CEW model can be longer; this means that mass transfer between the binary components is somewhat more stable for the CEW model than for the OTW model. This phenomenon is mainly caused by the different treatment of the mass-growth rate of the CO WD; i.e. the mass-growth rate during the CE evolution phase in the CEW model is higher than that during the OTW phase in the OTW model. So, for a given binary system, the WD mass (the mass ratio, $M_2/M_{\rm WD}$) at the same evolutionary stage for the CEW model is slightly higher (smaller) than in the OTW model, which leads to relatively more stable mass transfer for the CEW model. Especially in the right-upper part of the allowed parameter space for the CEW model, the systems will experience nova explosions, preventing the CO WD from reaching 1.378 $\rm M_\odot$ for the OTW model, while the WD will reach 1.378 $\rm M_\odot$ in the CE phase for the CEW model. This difference arises from the fact that the CE acts as a mass reservoir that can continuously feed material to the WD as long as the CE exists, even when $|\dot{M}_2| < \dot{M}_{\rm cr}$ as shown in Fig. 4.

Another difference is the minimum initial mass of CO WDs, $M_{\rm WD}^{\rm min}$, that can lead to SNe Ia. Previous studies showed that the minimum initial mass may be as low as 0.67 $\rm M_\odot$ for $Z = 0.02$ based on the OTW model (Langer et al. 2000; Han & Podsiadlowski 2004), and Meng et al. (2009a) found that $M_{\rm WD}^{\rm min}$ strongly depends on metallicity. Here, the minimum mass of CO WDs for $Z = 0.02$ is 0.65 $\rm M_\odot$, slightly lower than that for the OTW model, which is also a direct consequence of the different treatment of the mass-growth rate of the WDs.

These differences between the CEW model and the OTW model already indicate that the birth rate of SNe Ia in the CEW model should be somewhat higher than in the OTW model (see Section 5).

3.4 The final state of the systems

In this section, we examine the final state of the binary systems and the properties of the companions at the time of the SN explosion (assumed to occur when the WD mass has reached $M_{\rm WD} = 1.378\,{\rm M}_\odot$); this may be helpful for identifying SN Ia progenitor systems or for finding surviving companions in SN remnants.

3.4.1 Final contour

Fig. 9 shows the final states of binary systems leading to SNe Ia in the ($\log P^{\rm f} - M_2^{\rm f}$) plane when $M_{\rm WD} = 1.378\,{\rm M}_\odot$ for different initial WD masses, while Fig. 10 compares the initial and final contours of these systems. Generally, for a system with given initial parameters, the companion is still massive enough to maintain a high mass-transfer rate at the moment when $M_{\rm WD} = 1.378\,{\rm M}_\odot$. For example, many systems are still in the CEW phase at this moment; this means that the WDs in these systems would continue to increase their masses if the WDs did not explode at this stage. Even for the systems exploding in the SSS or RN phase, the companions may still be massive enough to maintain a high mass-transfer rate,

Downloaded from https://academic.oup.com/mnras/article-abstract/469/4/4763/3820926
by Said Business School user
on 16 February 2018

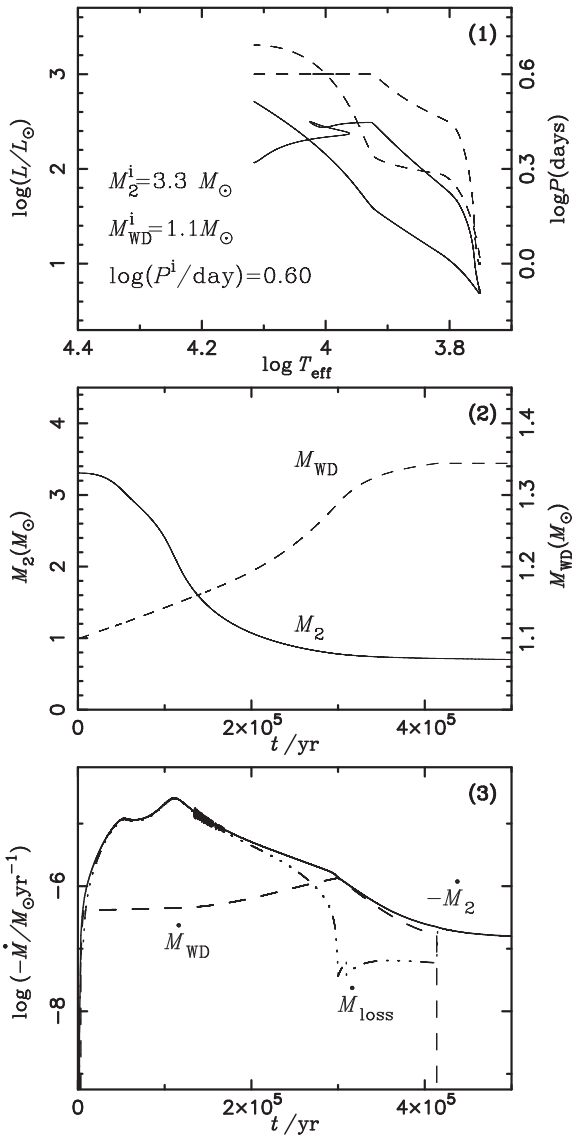

Figure 5. Similar to Fig. 3 but for different initial binary parameters.

so that the WDs could continue to grow in mass if they did not explode when $M_{WD} = 1.378\,M_\odot$ (see Figs 2 and 9). In other words, if the WD of a system is slightly less massive than 1.378 $M_\odot$ and its companion mass and orbital period are also located in the final contours for SNe Ia, it is still very likely for the WD to continue to increase its mass to 1.378 $M_\odot$. Fig. 10 shows that the positions of the final contours are below those of the initial contours; the secondary always has a mass less than 2.6 $M_\odot$, but can be as low as 0.6 $M_\odot$. Almost all models have a final orbital period between 0.22 and 6.5 d; these periods are generally shorter than in the OTW model (see Meng et al. 2009c). Similar to the initial contours, the parameter range of the final contours shrinks with decreasing initial WD mass and disappears when $M_{WD} = 0.65\,M_\odot$. An SSS (RX J0513.9−6951) and three RNe (CI Aql, U Sco and V394 CrA) are also indicated in Fig. 10 and two RNe (U Sco and V394 CrA) in Fig. 9. These objects have been considered good candidates for progenitor systems of SNe Ia as they contain massive WDs and have short orbital periods (Parthasarathy et al. 2007). Numerical simulations provide further support for the SN Ia progenitor connection (see below). RX J0513.9−6951 (open star) with $M_{WD} = 1.30\,M_\odot$ (Hachisu & Kato 2003b) is located within the initial contour for SN Ia progenitors. If the WD is a CO WD, it would make an excellent candidate for an SN Ia progenitor, as already suggested in Hachisu & Kato (2001) and Hachisu & Kato (2003b). For CI Aql, Sahman et al. (2013) recently analysed time-resolved, intermediate-resolution spectra during quiescence and found a WD mass of 1.00 $\pm$ 0.14 $M_\odot$ and a secondary mass of 2.32 $\pm$ 0.19 $M_\odot$. The position of CI Aql is also perfectly placed within the initial contours for SNe Ia. Even considering the uncertainty in the WD mass, our model suggests that CI Aql is another excellent SN Ia progenitor candidate system.

The dynamical mass estimates for the binary components in U Sco are $M_{WD} = 1.55 \pm 0.24\,M_\odot$ and $M_2 = 0.88 \pm 0.17\,M_\odot$ (Thoroughgood et al. 2001), while model simulations show U Sco to be a WD + MS system with $M_{WD} = 1.37\,M_\odot$ and $M_2 = 1.5\,M_\odot$, although a mass between 0.8 and 2.0 $M_\odot$ is also acceptable (Hachisu et al. 2000a,b, see also the binary evolution model in Podsiadlowski 2003). Both the dynamical estimates and model simulations indicate that the mass of the WD in U Sco is quite close to 1.378 $M_\odot$. Figs 9 and 10 that show that U Sco is well located within the final contours for SNe Ia, irrespective of whether the companion mass is taken from model simulations or dynamical estimates; this suggests that the companion has enough material to maintain a high mass-transfer rate to increase the WD mass to 1.378 $M_\odot$. Therefore, our model supports the previous suggestion that, if the WD in U Sco is a CO WD, it is an excellent candidate for an SN Ia progenitor. However, whether or not the massive WD is a CO or an ONeMg one is still under debate (Mason 2011; Kato & Hachisu 2012). Further effort, both on the observational and the theoretical side, is clearly needed to decide the fate of U Sco. The WD mass of V394 CrA has been estimated to be 1.37 $M_\odot$, while the mass of the companion is still unclear. The best-fitting companion mass for this recurrent nova system is 1.50 $M_\odot$, while a mass between 0.8 and 2.0 $M_\odot$ is still acceptable (Hachisu & Kato 2000, 2003a; Hachisu, Kato & Schaefer 2003). In either case, it is still very likely that the WD can increase its mass to 1.378 $M_\odot$. Assuming a CO composition for the WD of V394 CrA, our results confirm that it provides an excellent candidate for an SN Ia progenitor. In any case, further observations are necessary to determine the masses of the WD and the secondary in V394 CrA.

In addition, as the well candidates of the progenitors of SNe Ia, U Sco and V394 CrA provide an opportunity to examine the progenitor models of SNe Ia in a detailed way, i.e. whether or not the two RNe may locate in the RN region for SNe Ia predicted by any successful SD model. In Fig. 9, although the expected regions for the CEW, SSS and RN phases overlapped each other, the RN region predicted by our CEW model may explain the positions of U Sco and V394 CrA in the (log $P^f - M_2^f$) plane. According to Fig. 9, both U Sco and V394 CrA are likely to come from systems with an initial WD mass between 1.0 and 1.1 $M_\odot$ if the best-fitting companion masses from model simulations are taken, while the dynamical estimate for U Sco favours a system with $M_{WD}^i \leq 0.9\,M_\odot$.

3.4.2 *Mass and orbital velocity*

In Fig. 11, we show the parameter regions for the companion mass and its orbital velocity when $M_{WD} = 1.378\,M_\odot$ for different initial WD masses. The ranges of companion mass and orbital velocity here are very similar to those shown in Han (2008) and Meng & Yang (2010b) although their results were based on the OTW model. At the time of the SN, the companion mass lies between 0.6 and 2.6 $M_\odot$ and the orbital velocity between 60 and 260 km s^{-1}. The

Downloaded from https://academic.oup.com/mnras/article-abstract/469/4/4763/3820926
by Said Business School user
on 16 February 2018

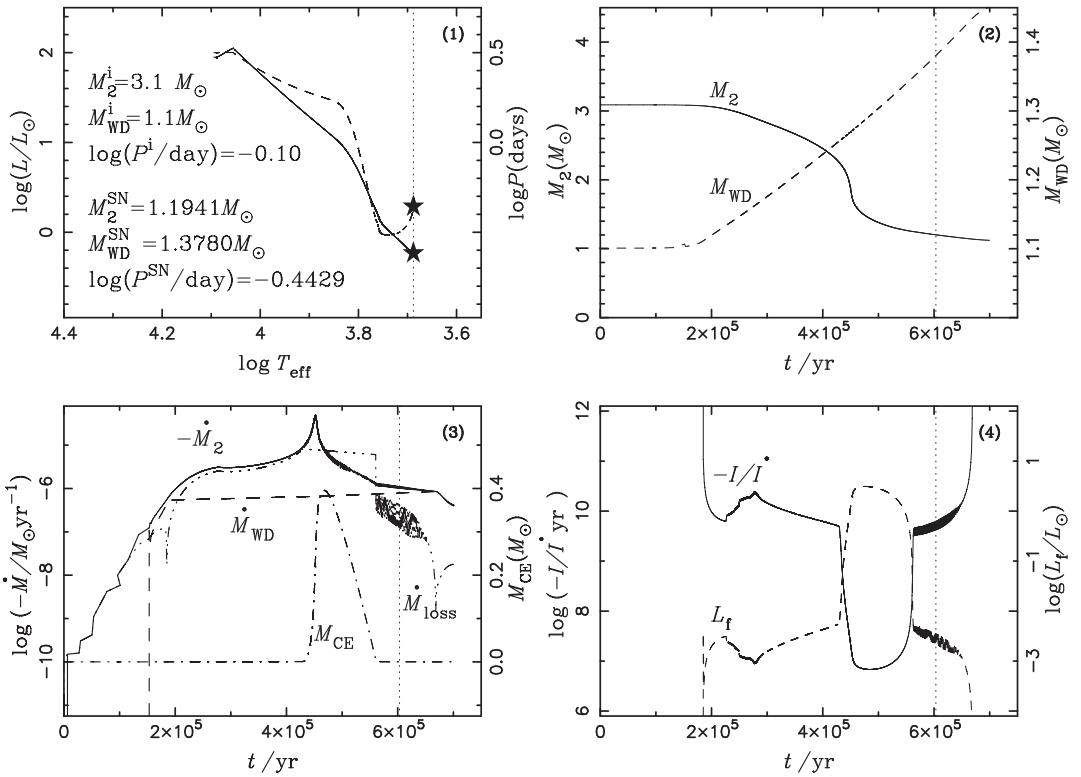

Figure 6. Similar to Fig. 2 for different initial binary parameters, illustrating a relatively extreme case.

impact of the SN ejecta with the envelope of the companion may strip off some hydrogen-rich material from the surface of the companion. At the same time, the companion may receive a velocity kick, i.e. the final space velocity of a surviving companion in an SN remnant is $v_{\rm s} = \sqrt{v_{\rm orb}^2 + v_{\rm kick}^2}$ (Marietta, Burrows & Fryxell 2000; Meng, Chen & Han 2007; Pakmor et al. 2008; Liu et al. 2012). Generally, the stripped-off material is much less massive than the companion, and the kick velocity is much smaller than the orbital velocity. In any case, the companion mass and its orbital velocity here should be taken as upper and lower limits for the mass and the space velocity of the surviving companion in an SN remnant, respectively. In the figure, we also plotted the parameters for the potential surviving companion of Tycho's SN (Tycho G, Ruiz-Lapuente et al. 2004; González-Hernández et al. 2009; Bedin et al. 2014). Although it is presently unclear whether Tycho G actually is the surviving companion (see the discussion in Section 3.4.3), its claimed parameters would be compatible with the range of the companion mass and its orbital velocity presented here.

3.4.3 *Companion radius and rotational velocity*

In Fig. 12, we present the parameter regions for the companion radius and its equatorial rotational velocity when $M_{\rm WD} = 1.378\,{\rm M}_\odot$ for different initial WD masses. In our calculations, we did not keep track of the companion radius as it can be obtained by some simple assumptions. We assume that the companion radius is equal to its Roche lobe radius, i.e. the companion is filling its Roche lobe at the moment of the SN explosion, and the donor's radius will not be far away from that shown in Fig. 12. The equatorial rotation velocity is calculated assuming that the companion star corotates with the orbit. The figure shows that the rotational velocity of the surviving companions ranges from 40 to 220 km s^{-1}; this means that, in many cases, the companions' spectral lines should be noticeably broadened if the rotation of the star is not affected by the impact of the SN ejecta. We note that the upper limit of the rotational velocity here is higher than that based on the OTW model in Han (2008) (170 km s^{-1}) since the final orbital periods tend to be shorter in the CEW model than in the OTW model (see Figs 2 and 3). The companion radius lies between 0.5 and 9 $\rm R_\odot$. In general, the companion stars with larger radii have lower rotational velocities. This figure may be helpful for identifying the companion nature of a potential surviving candidate in an SN remnant. However, although the radius of Tycho G (1–3 $\rm R_\odot$) matches well with our calculations, its rotational velocity is much smaller than predicted here; this is the reason why Kerzendorf et al. (2009) have strongly argued against Tycho G being the surviving companion of Tycho's SN. Here, we do not consider the impact of the SN ejecta on the companion. If the companion expands significantly because of the impact, its rotational velocity will be significantly reduced. Indeed, as argued by Kerzendorf et al. (2009) (also see Meng & Yang 2011a), it is possible in principle to explain the observed rotational velocity in Tycho G if the companion's envelope was almost completely stripped by the SN impact and the surface layers we see now had to expand from regions near the core. These expectations, that follow from simple angular-momentum conservation considerations, have been confirmed by numerical simulations (e.g. Pan, Ricker & Taam 2012a; Liu et al. 2013), though we note that none of the simulations in Pan et al. (2012a) can explain the observed properties of Tycho G as none can fit the observed gravity ($\log g$) and the observed rotational velocity simultaneously.

3.4.4 *Luminosity and effective temperature*

Fig. 13 shows the parameter regions for the luminosity and the temperature of the companion when $M_{\rm WD} = 1.378\,{\rm M}_\odot$ for different initial WD masses. The luminosity ranges from 0.25 to 100 $\rm L_\odot$,

Downloaded from https://academic.oup.com/mnras/article-abstract/469/4/4763/3820926
by Said Business School user
on 16 February 2018

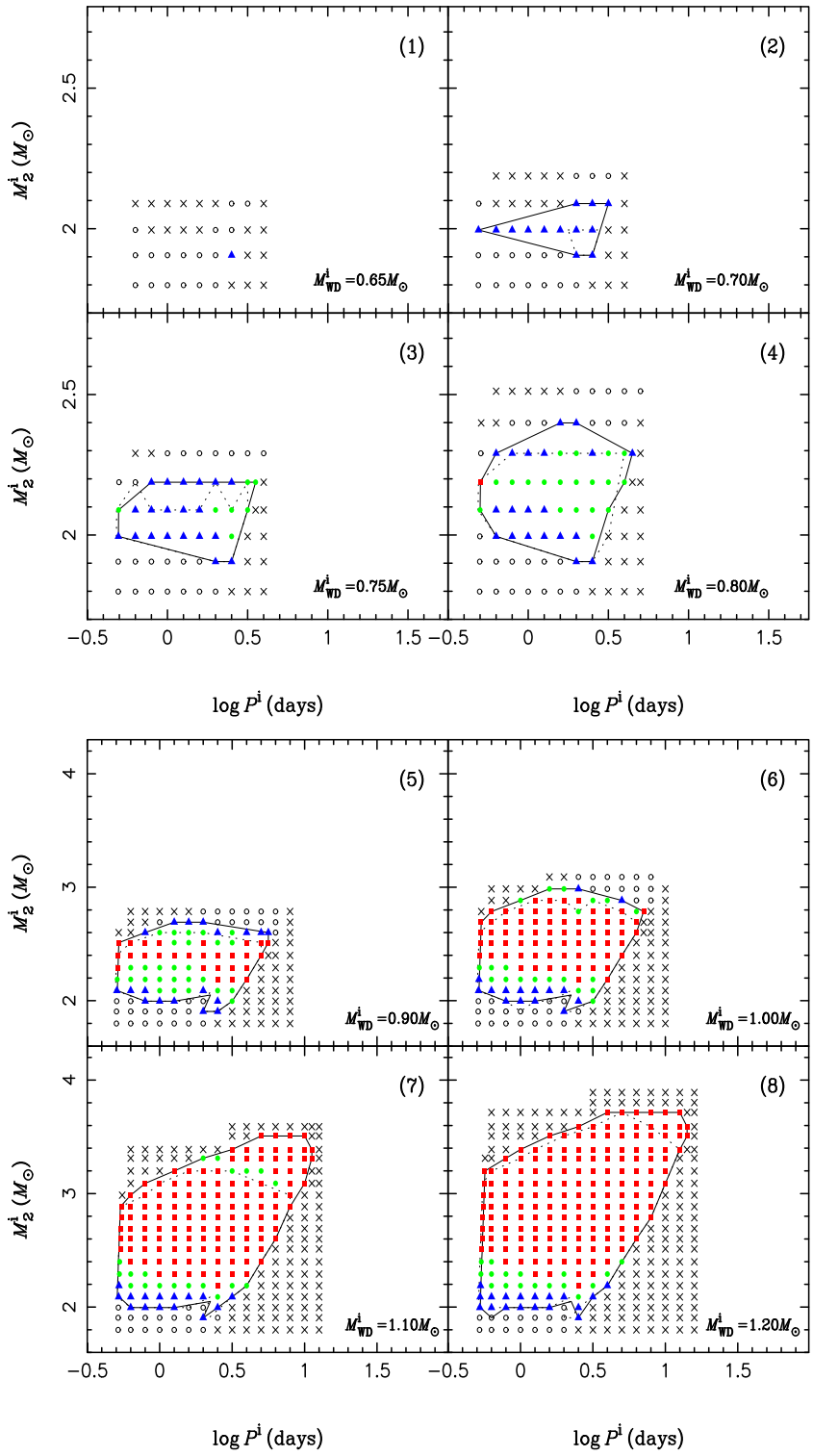

Figure 7. Final outcomes of the binary evolution calculations in the CEW model in the initial orbital period – secondary mass (log $P^{\rm i}$, $M_2^{\rm i}$) plane, where $P^{\rm i}$ is the initial orbital period, and $M_2^{\rm i}$ is the initial mass of the donor star (for different initial WD masses as indicated in each panel). Filled squares indicate SN Ia explosions during a CE phase ($M_{\rm CE} > 0$). Filled circles denote that SN Ia explosions occur in the SSS phase ($\dot{M}_{\rm cr} \geq |\dot{M}_2| \geq \frac{1}{2}\dot{M}_{\rm cr}$ and $M_{\rm CE} = 0$), while filled triangles denote that SN Ia explosions occur in the RN phase ($\frac{1}{2}\dot{M}_{\rm cr} > |\dot{M}_2| \geq \frac{1}{8}\dot{M}_{\rm cr}$ and $M_{\rm CE} = 0$). Open circles indicate systems that experience nova explosions, preventing the CO WD from reaching 1.378 $M_\odot$ ($|\dot{M}_2| < \frac{1}{8}\dot{M}_{\rm cr}$ and $M_{\rm CE} = 0$), while crosses show the systems that are unstable to dynamical mass transfer. The solid curves show the contours of the parameter space leading to SNe Ia for the CEW model, while, for comparison, the dotted curves show the contours from the OTW model (taken from Meng et al. 2009a).

Downloaded from https://academic.oup.com/mnras/article-abstract/469/4/4763/3820926
by Said Business School user
on 16 February 2018

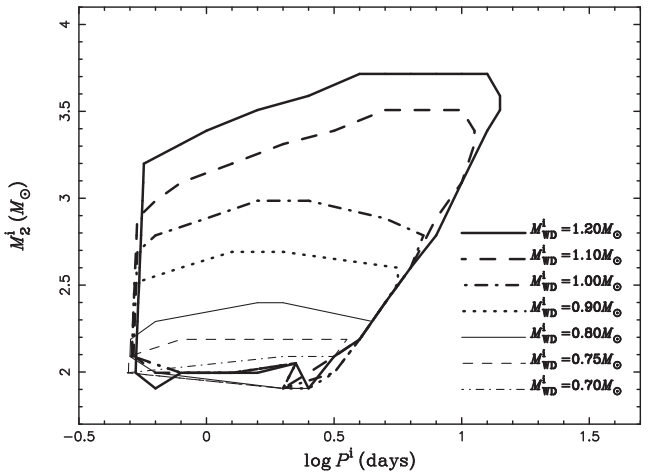

Figure 8. The contours of initial parameters in the (log P^i, M_2^i) plane for different initial WD masses for which SNe Ia are expected. For $M^i_{WD} = 0.65\,M_\odot$, the contour shrinks to a point and is not included in the figure.

and the effective temperature from 4470 to 12 600 K. The range of effective temperatures is slightly larger than in the OTW model (Han 2008), which again is a direct consequence of the different treatment of the mass-growth rate of the WD, leading to a larger initial parameter space in the initial secondary mass–orbital period plane.

The luminosity and the effective temperature of a companion will generally be affected by the impact of the SN ejecta (Marietta et al. 2000; Podsiadlowski 2003; Shappee, Kochanek & Stanek 2013); hence, Fig. 13 can only give an indication for the initial conditions when exploring the evolution and appearance of a companion star during the post-impact re-equilibration phase when the star is out of thermal equilibrium. Podsiadlowski (2003) calculated the luminosity evolution of a subgiant star of 1 $M_\odot$ after being hit by the ejecta of an SN Ia and found that the luminosity evolution was initially much faster than the Kelvin–Helmholtz time-scale of the pre-SN subgiant since the re-equilibration time-scale is determined by the thermal time-scale of the outer layer of the star, which can be many orders of the magnitude shorter. Depending on the amount of energy deposited, the luminosity of the companion may be either significantly overluminous or underluminous (0.1–200 $L_\odot$) 440 yr after the SN explosion. Pan, Ricker & Taam (2012b) found that the evolution of the remnant star strongly depends not only on the amount of energy deposited from the explosion but also on the depth of the energy deposition and that the luminosity of the remnant could be close to that of Tycho G ∼500 yr after the explosion (consistent with the conclusions of Podsiadlowski 2003). Shappee et al. (2013) calculated the future evolution of the companion by injecting (2–6) × 10^{47} erg of energy into the stellar-evolution model of a 1 $M_\odot$ donor star and found that the companion becomes significantly more luminous (10–10^3 $L_\odot$) for a long period of time (10^3–10^4 yr) due to the Kelvin–Helmholtz collapse of the envelope. These simulations and our binary evolution calculations partly share the luminosity range, especially for the results in Podsiadlowski (2003). The potential surviving companion of Tycho's SN is well located within the contour of Fig. 13. However, as we discussed in Section 3.4.3, no model to date can reproduce log g, the rotation velocity and the luminosity of Tycho G simultaneously. Observations are also not fully conclusive. While Bedin et al. (2014) in their reanalysis conclude that the proper motion and chemical abundance of Tycho G are consistent with it being a surviving companion, Xue & Schaefer (2015), measuring the exact explosion site of Tycho's SN, found that Tycho G is outside the 1σ error region (7.3 arcsec) at very high significance. Therefore, Tycho G may just be a Milky Way thick-disc star that happens to pass in the vicinity of the SN remnant (Fuhrmann 2005; but also see Bedin et al. 2014 for a different view).

3.4.5 *Mass loss*

Fig. 14 shows the mass-lose rate from the system and the total amount of material lost when $M_{WD} = 1.378\,M_\odot$. Here, the CE mass is included in the material lost since the CE material may generally be lost eventually (see the further discussion in Section 6.1) or provide a mass reservoir to form a circumbinary disc. This assumption for the material lost is reasonable for about 99 per cent of all SNe Ia, because the CE mass is so small (less massive than ∼10^{-3} $M_\odot$) for most SNe Ia exploding in the CE phase. Only for the cases of $M^i_{WD} \geq 1.1\,M_\odot$, may this assumption affect the upper parts of the contours, i.e. the upper limit of the amount of the lost material may be overestimated by a few tenths $M_\odot$ if one assumes that the CE contributes to the lost material. As Fig. 14 shows, the mass-loss rate covers three orders of magnitude, i.e. from ∼10^{-8} to 10^{-5} $M_\odot$ yr^{-1}. The lower limit of the mass-loss rate for the CEW model is mainly constrained by the mass loss during helium shell burning, while the upper limit is mainly determined by the Eddington luminosity. The lower mass-loss rate from systems in the CEW model may help to explain why the circumstellar environment contains very little mass around some SNe Ia such as SN 2011fe (Patat et al. 2013), although there are ongoing arguments on whether SN 2011fe originates from an SD or a DD system (Li et al. 2011b; Chomiuk 2013; Mazzali et al. 2014; Meng & Han 2016).

In our model, a large amount of material may be lost from the CE surface: it may be as large as 2.5 $M_\odot$. This could be the cause of the colour excess seen in SNe Ia (Meng et al. 2009b). As this material cools, part of it may form dust and cause light echoes (Wang et al. 2008; Yang et al. 2017). The dust should be distributed over a large region around SNe Ia, where the extent should be smaller than the maximum distance that the lost material can reach. Fig. 15 shows the contour of the total amount of material lost from the system and the maximum distance that the lost material may reach by the time when $M_{WD} = 1.378\,M_\odot$. The maximum distance is simply $d = v_w \times t_d$, where v_w is the wind velocity[7] of the material lost, here assumed to be 50 km s^{-1}, and t_d is the delay time from the onset of mass transfer to the moment when $M_{WD} = 1.378\,M_\odot$. There is a trend in Fig. 15 that the maximum distance is closer if a larger amount of material is lost. This is caused by the effect of the initial WDs and the companions on the mass-transfer time-scale: for a lower initial WD mass and a lower companion mass, the mass-transfer time-scale for increasing the WD to 1.378 $M_\odot$ is longer, and the wind material can reach a larger distance. At the same time,

[7] For the present CEW model, the exact value of the CEW velocity is still quite uncertain, but a value larger than that of an AGB star may be expected. For example, the wind velocity for an AGB star with a core of 0.8 $M_\odot$ and an envelope of 0.1 $M_\odot$ is very likely to be smaller than that of a system with a CO WD of 0.8 $M_\odot$ and a companion of ∼2.0 $M_\odot$ covered by a CE of 10^{-3} $M_\odot$, e.g. the system shown in Fig. 2, due to a higher escape velocity from the surface of the CE. In addition, a value of $\leq 100\,km\,s^{-1}$ for the outflow from the SD systems is also consistent with the dynamics of the forward shock and the X-ray emission from the shocked SN ejecta in some SNRs (Badenes et al. 2007).

Downloaded from https://academic.oup.com/mnras/article-abstract/469/4/4763/3820926
by Said Business School user
on 16 February 2018

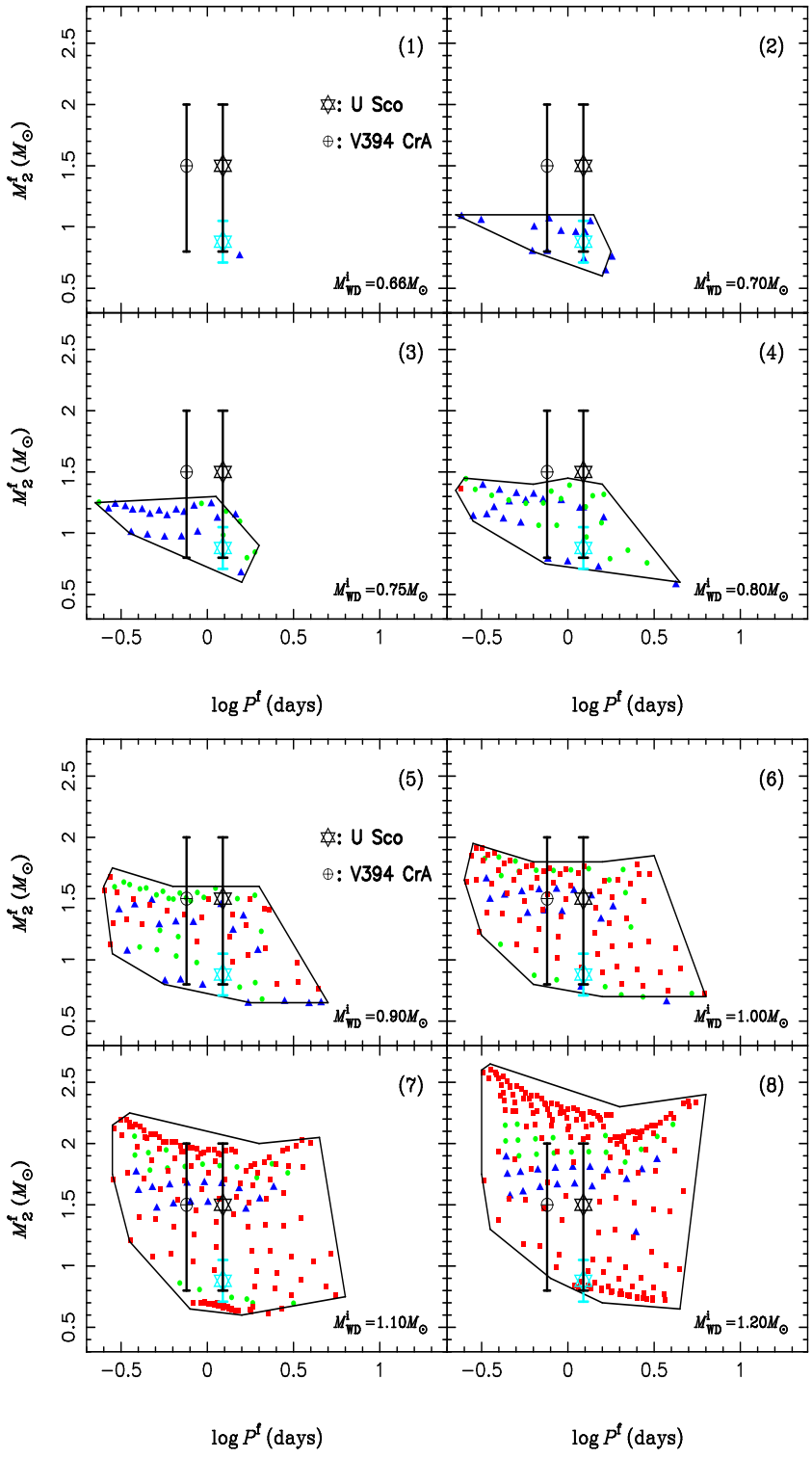

Figure 9. Similar to Fig. 7 but for the final state of the binary systems in the CEW model in the final orbital period – secondary mass ($\log P^{\rm f}$, $M_2^{\rm f}$) plane, where $P^{\rm f}$ is the final orbital period, and $M_2^{\rm f}$ is the final mass of the donor star (for different initial WD masses as indicated in each panel) at the moment of $M_{\rm WD}=1.378\,{\rm M}_\odot$. Filled squares indicate SN Ia explosions during a CE phase ($M_{\rm CE}>0$). Filled circles denote that SN Ia explosions occur in the SSS phase ($\dot{M}_{\rm cr}\geq|\dot{M}_2|\geq\frac{1}{2}\dot{M}_{\rm cr}$ and $M_{\rm CE}=0$), while filled triangles indicate that SN Ia explosions occur in the RN phase ($\frac{1}{2}\dot{M}_{\rm cr}>|\dot{M}_2|\geq\frac{1}{8}\dot{M}_{\rm cr}$ and $M_{\rm CE}=0$). The solid curves show the contours of the parameter space. Two recurrent novae are indicated by a hexagram for U Sco and an Earth symbol for V394 CrA, where the position of the black hexagram is based on the model simulation by Hachisu et al. (2000a,b), while the bright blue hexagram taken from the dynamical estimate (Thoroughgood et al. 2001).

Downloaded from https://academic.oup.com/mnras/article-abstract/469/4/4763/3820926
by Said Business School user
on 16 February 2018

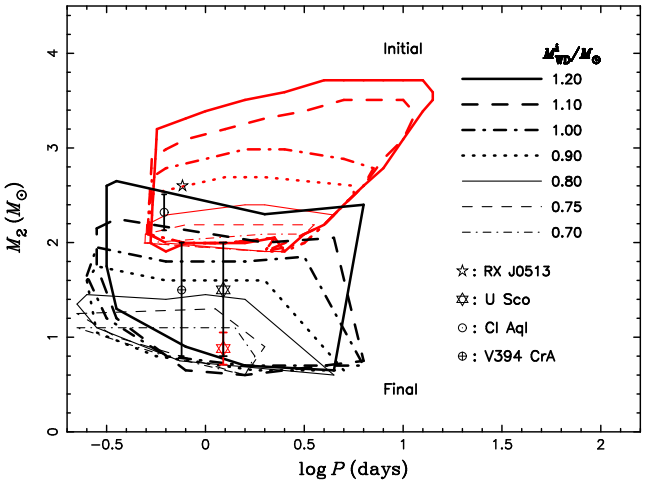

Figure 10. Parameter regions producing SNe Ia in the (log P–M_2) plane for WD + MS systems with different initial WD masses in the CEW model. In the WD + MS systems inside the region enclosed by the red curves (labelled 'initial'), the white dwarf is able to grow to a mass of 1.378 $M_\odot$, where an SN Ia explosion is assumed to occur. The final state of the WD + MS systems is enclosed by the black curves (labelled 'final'). A supersoft X-ray source, RX J0513.9−6951 (open star) is also plotted; its orbital period is 0.763 d (Pakull et al. 1993). Three recurrent novae are indicated by a hexagram for U Sco (with a period of 1.2306 d; Schaefer & Ringwald 1995; Hachisu et al. 2000a,b), a solar symbol for CI Aql (with an orbital period of 0.6184 d; Mennickent & Honeycut 1995; Sahman et al. 2013) and an Earth symbol for V394 CrA (with an orbital period of 0.7577 d; Schaefer 1990), where the black hexagram assumes the companion mass from the model simulation by Hachisu et al. (2000a,b), while the red hexagram takes it from the dynamical estimate (Thoroughgood et al. 2001).

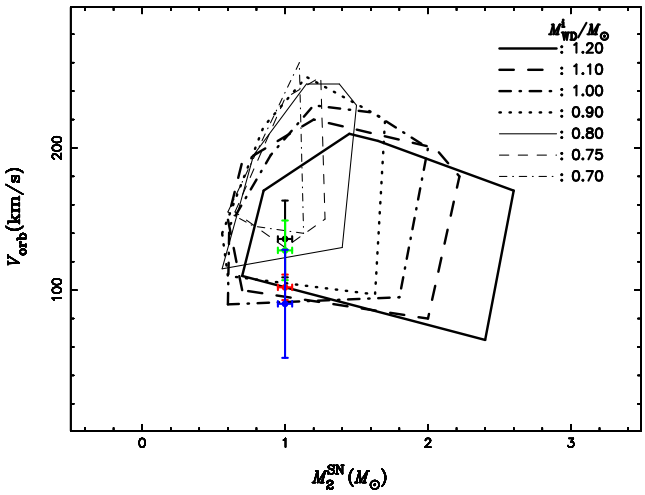

Figure 11. Parameter space for the companion mass and its orbital velocity when $M_{WD} = 1.378\,M_\odot$ for different initial WD masses in the CEW model. The cross represents the potential companion of Tycho's SN progenitor, Tycho G, and the length of the cross indicates the typical observational errors, where the space velocities for Tycho G are taken from Ruiz-Lapuente et al. (2004) (black), González-Hernández et al. (2009) (green), Kerzendorf et al. (2009) (blue) and Bedin et al. (2014) (red).

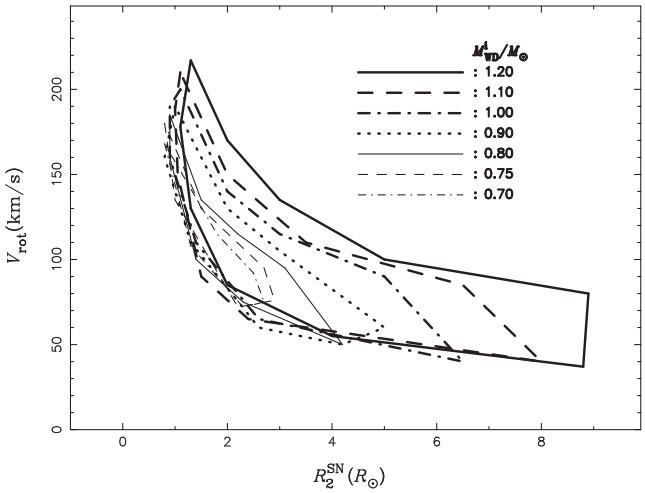

Figure 12. Parameter regions for the companion radius and its equatorial rotational velocity when $M_{WD} = 1.378\,M_\odot$ for different initial WD masses in the CEW model.

a less massive companion means a lower mass-transfer rate and consequently much lower mass-loss rate, which results in a smaller amount of the lost material although the mass-transfer time-scale is longer. In particular, for some SNe Ia, the amount of lost material is quite small (no more than 0.2 $M_\odot$), but is spread over a very large scale (∼300 pc). In these cases, the environment around the SNe Ia should be very clean. In a follow-up paper, we will discuss the observational consequences of these properties in a detailed BPS study.

We must emphasize that the results from Fig. 10 to Fig. 15 are based on the assumption that the WD explodes as a SN Ia when its mass reaches 1.378 $M_\odot$. However, the explosion could be delayed if the WD is rotating rapidly (see the discussion in Section 5.2), in which case the final state of the binary system could be quite different from what is presented here. For example, the range of the companion mass should move to a lower value and the range of the final orbital period may be increased, i.e. range from a value lower than 0.2 d to one longer than 6.5 d. Similarly, the range of the radius, rotation velocity and orbital velocity are also increased, i.e. the lower boundary moves to a lower value while the upper boundary moves to a higher value. As a consequence, $M_{\rm lost}$ would be larger, while the final mass-loss rate from the binary system would be lower, producing a cleaner environment around the SN Ia.

4 BINARY POPULATION SYNTHESIS

Adopting the results in Section 3, we have estimated the expected SN frequency from the WD+MS channel using the rapid binary evolution code developed by Hurley, Pols & Tout (2000); Hurley, Tout & Pols (2002). Hereafter, we use *primordial* to refer to the binaries before the formation of the WD+MS systems and *initial* for the WD+MS systems (see also Meng et al. 2009a and Meng & Yang 2010a).

4.1 Common-envelope evolution

In the evolution of a binary, the primordial mass ratio (the ratio of the mass of the primary to the mass of the secondary) is crucial for the nature of the first mass-transfer phase. There is a critical mass ratio, $q_{\rm c}$, which determines the evolutionary direction of a binary system. If the primordial mass ratio is larger than $q_{\rm c}$, the system will experience dynamically unstable mass transfer and the system

Downloaded from https://academic.oup.com/mnras/article-abstract/469/4/4763/3820926
by Said Business School user
on 16 February 2018

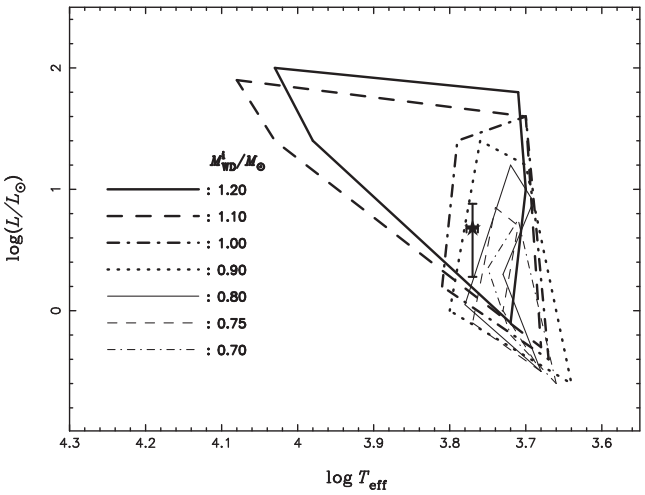

Figure 13. The parameter regions for the luminosity and the temperature of the companion when $M_{WD} = 1.378\,M_\odot$ for different initial WD masses. The star represents the potential surviving companion star of Tycho's SN, Tycho G, where the bar represents the observational error (Ruiz-Lapuente et al. 2004).

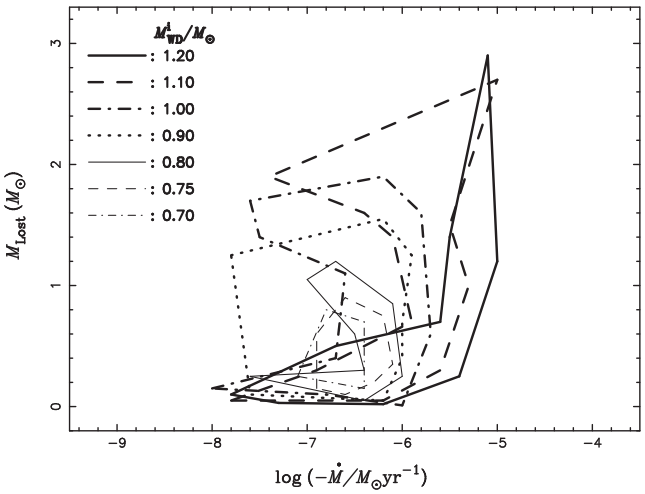

Figure 14. The parameter regions for the mass-loss rate and the total amount of material lost from the system when $M_{WD} = 1.378\,M_\odot$ for different initial WD masses, where the CE mass is included in the amount of material lost from the system.

will enter into a CE phase[8] (Paczyński 1976). The value of q_c is a function of the evolutionary state of the primordial primary at the onset of RLOF (Hjellming & Webbink 1987; Webbink 1988; Han et al. 2002; Podsiadlowski, Rappaport & Pfahl 2002; Chen & Han 2008). In this paper, we set $q_c = 4.0$ if the primary fills its Roche lobe on the MS or in the HG. Such a value is supported by various detailed binary evolution studies (Han et al. 2000; Chen & Han 2002, 2003). If the primordial primary fills its Roche lobe on the first giant branch (FGB) or AGB, we adopt

$$q_c = \left[1.67 - x + 2\left(\frac{M^P_{c1}}{M^P_1}\right)^5\right]/2.13, \quad (18)$$

[8] Note that the CE here forms on a dynamical time-scale while the CE in our CEW model is maintained on a thermal time-scale.

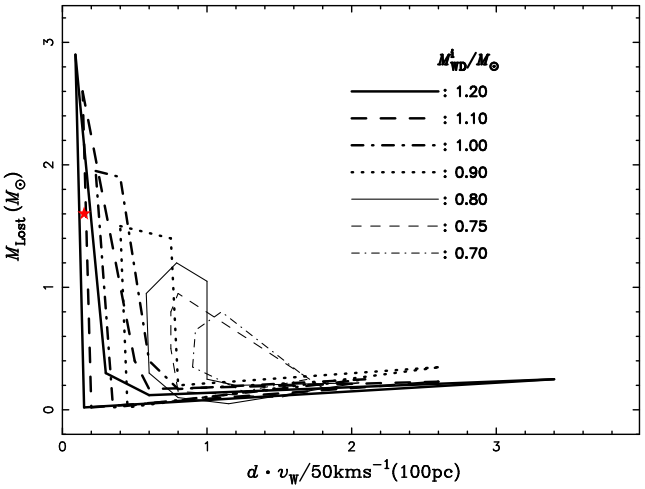

Figure 15. The parameter regions for the total amount of material lost from the system and the maximum distance that the lost material may reach by the time when $M_{WD} = 1.378\,M_\odot$ for different initial WD masses; here, the CE mass is included in the amount of material lost from the system. The red star represents the Galactic SN remnant RCW 86 (Broersen et al. 2014).

where M^P_{c1} is the core mass of the primordial primary, and $x = \mathrm{d}\ln R^P_1/\mathrm{d}\ln M^P_1$ is the mass–radius exponent of the primordial primary, where $x \simeq 0.3$ and changes with the stellar composition. If the mass donors (primaries) are naked helium giants, we take $q_c = 0.748$ (see details in Hurley et al. 2002).

The 'new' binary embedded in the CE consists of the dense core of the primordial primary and the primordial secondary and will lose its orbital energy due to the friction between the CE and the binary system. A part of the orbital energy released by the system during the spiral-in process is injected into the envelope to eject the material in the CE (Livio & Soker 1988). In this paper, we assume that the CE is ejected completely if

$$\alpha_{CE}\Delta E_{orb} = |E_{bind}|, \quad (19)$$

where E_{bind} is the binding energy of the CE, ΔE_{orb} is the orbital energy released during the spiral-in phase and α_{CE} denotes the CE ejection efficiency (i.e. the fraction of the released orbital energy that can be used in ejecting the CE). Since the internal energy and, in particular, the recombination energy in the envelope is not incorporated in the binding energy (Ivanova et al. 2013; Ivanova, Justham & Podsiadlowski 2015), α_{CE} can be larger than 1 (see Han, Podsiadlowski & Eggleton 1995 on the discussion of the internal energy). Here, $\alpha_{CE} = 1.0$ or $\alpha_{CE} = 3.0$ is adopted.

4.2 Evolutionary channels for WD + MS systems

There are three evolutionary channels to form WD + MS systems based on the evolutionary state of the primordial primary at the onset of the first RLOF.

Case 1 (He star channel): the primordial primary is in the HG or on the RGB at the onset of the first RLOF phase (so-called case B evolution as defined by Kippenhahn & Weigert 1967). In this case, a CE forms either because of a large mass ratio or because the mass donor has a deep convective envelope. After CE ejection, the system consists of a helium star and an MS star. The helium star continues to evolve and will fill its Roche lobe again after helium has been exhausted in the centre. Due to the small mass ratio, mass transfer is dynamically stable leading to the formation a close CO WD + MS system (see Nomoto et al. 1999, 2003 for details).

Downloaded from https://academic.oup.com/mnras/article-abstract/469/4/4763/3820926
by Said Business School user
on 16 February 2018

Case 2 (EAGB channel): the primordial primary is on the early AGB stage (EAGB) (i.e. helium is exhausted in the core, while thermal pulses have not yet started). At this stage, the hydrogen-exhausted core, i.e. the CO core surrounded by a dense helium shell, is much denser than the hydrogen-rich envelope, and there is a steep gradient in the gravitational potential between the hydrogen-exhausted core and the hydrogen-rich envelope (e.g. fig. 2 in Meng, Chen & Han 2008). If the system experiences dynamically unstable mass transfer, the system will enter a CE and spiral-in phase where the hydrogen-rich envelope forms a CE. After the ejection of the CE, the new, much closer binary consists of the hydrogen-exhausted core and the secondary. Eventually the primordial primary becomes a helium red giant and may fill its Roche lobe to start a second phase of RLOF. Similarly to the He star channel, this RLOF phase is stable and produces WD + MS systems after the end of RLOF.

Case 3 (TPAGB channel): the primordial primary fills its Roche lobe during the TPAGB stage. Similarly to the above two channels, a CE is formed during the first RLOF phase. A CO WD + MS binary is produced after CE ejection.

The WD + MS systems continue to evolve, and the MS companions will, at some stage, fill their Roche lobes and transfer matter to the CO WDs, which may subsequently explode as SNe Ia. Here, we assume that, if the initial orbital period, $P^{\rm i}_{\rm orb}$, and the initial secondary mass, $M^{\rm i}_2$, of a WD + MS system are located in the appropriate region in the ($\log P^{\rm i}$, $M^{\rm i}_2$) plane (see Fig. 7) for SNe Ia at the onset of RLOF, a SN Ia is produced.

4.3 Basic parameters for the Monte Carlo simulations

To investigate the birth rate of SNe Ia, we followed the evolution of 10^7 binaries using the Hurley rapid binary evolution code (Hurley et al. 2000, 2002). The results of the grid calculations in Section 3 are incorporated into the code. The primordial binary samples are generated in a Monte Carlo way, where circular orbits are assumed for all binaries. The basic parameters for the simulations are as follows:

(i) The initial mass function of Miller & Scalo (1979) is adopted. The primordial primary is generated according to the formula of Eggleton, Tout & Fitechett (1989)

$$M_1^{\rm p} = \frac{0.19X}{(1-X)^{0.75} + 0.032(1-X)^{0.25}}, \qquad (20)$$

where X is a random number in the range [0, 1], and $M_1^{\rm p}$ is the mass of the primordial primary, which is between 0.1 and 100 $\rm M_\odot$.

(ii) For the evolution of a binary system, the primordial mass ratio, q', is a crucial parameter as it determines the evolutionary direction of the system. In the paper, a uniform mass-ratio distribution is adopted, i.e. q' is uniformly distributed in the range [0, 1] (Mazeh et al. 1992; Goldberg & Mazeh 1994):

$$n(q') = 1, \qquad 0 < q' \leq 1, \qquad (21)$$

where $q' = M_2^{\rm p}/M_1^{\rm p}$.

(iii) All stars are assumed to be members of binary systems. For the separation of the binary systems, a constant distribution in $\log a$ is assumed for wide binaries, while a falls off smoothly for close binaries:

$$a \cdot n(a) = \begin{cases} \alpha_{\rm sep}(a/a_0)^{\rm m} & a \leq a_0; \\ \alpha_{\rm sep}, & a_0 < a < a_1, \end{cases} \qquad (22)$$

where $\alpha_{\rm sep} \approx 0.070$, $a_0 = 10\,\rm R_\odot$, $a_1 = 5.75 \times 10^6\,\rm R_\odot = 0.13\,pc$ and $m \approx 1.2$. The separation distribution adopted here implies an equal number of wide binary systems per logarithmic interval, and gives approximately 50 per cent of binary systems with an orbital period $\leq$100 yr (see also Han et al. 1995).

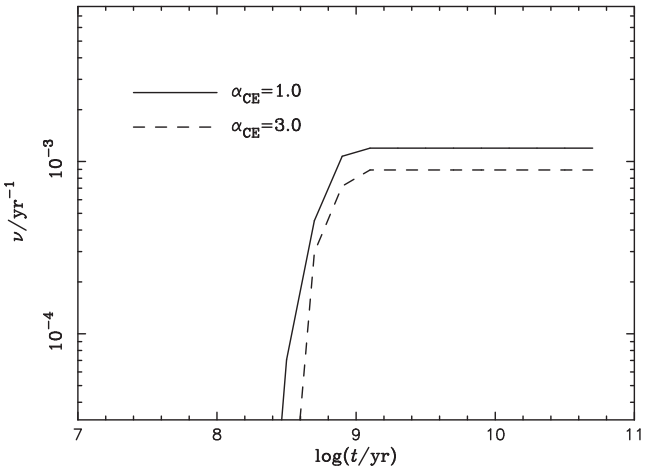

Figure 16. The evolution of the birth rates of SNe Ia for a constant SFR ($Z = 0.02$, SFR $= 5\,\rm M_\odot\,yr^{-1}$). The solid and dashed curves show the cases with $\alpha_{\rm CE} = 1.0$ and $\alpha_{\rm CE} = 3.0$, respectively.

(iv) We simply adopt either a single starburst (i.e. $10^{11}\,\rm M_\odot$ in stars is generated at a single instant of time) or a constant star formation rate (SFR) S for the last 15 Gyr. Here the value of S is set to be $5\,\rm M_\odot\,yr^{-1}$, which is calibrated to maintain the production of one binary with $M_1 > 0.8\,\rm M_\odot$ in the Galaxy every year (see Iben & Tutukov 1984; Han et al. 1995; Hurley et al. 2002; Willems & Kolb 2004). The value of $5\,\rm M_\odot\,yr^{-1}$ can successfully reproduce the birth rate of the core-collapse SN and the ^{26}Al 1.809 MeV gamma-ray line in the galaxy (Timmes, Diehl & Hartmann 1997).

5 BINARY POPULATION SYNTHESIS RESULTS

5.1 The birth rate

Fig. 16 shows the Galactic birth rates of SNe Ia (i.e. $Z = 0.02$ and SFR $= 5.0\,\rm M_\odot\,yr^{-1}$) from the WD+MS channel. The Galactic birth rate is around $(0.89–1.20)\times10^{-3}\,\rm yr^{-1}$, which is higher than that from the OTW model by about $\sim$30 per cent (see fig. 6 in Meng et al. 2009a), as one would expect since the parameter space for SNe Ia here is larger in our model than in the OTW model. This result is somewhat lower but still comparable to that inferred from observations ($3–7\times10^{-3}\,\rm yr^{-1}$, van den Bergh & Tammann 1991; Cappellaro & Turatto 1997; Li et al. 2011a).

The birth rate of SNe Ia for a single starburst is presented in Fig. 17. In this case, most SNe occur between 0.25 and 2 Gyr after the starburst. Similarly, the peak value here is also slightly higher than that from the OTW model (see fig. 7 in Meng et al. 2009a). In addition, Fig. 17 shows that a low $\alpha_{\rm CE}$ leads to a higher birth rate (see also Fig. 16), since a low value of $\alpha_{\rm CE}$ means that a primordial system needs to release more orbital energy to eject the CE for the formation of a WD + MS system; hence, the resulting WD + MS systems tend to have shorter orbital periods and thereby more easily fulfil the conditions for SNe Ia. In addition, only when $\alpha_{\rm CE}$ is low enough, may the WD + MS system produced from the TPAGB channel contribute to the SN Ia population (see also Meng et al. 2009a). Moreover, our CEW model may produce SNe with

Downloaded from https://academic.oup.com/mnras/article-abstract/469/4/4763/3820926
by Said Business School user
on 16 February 2018

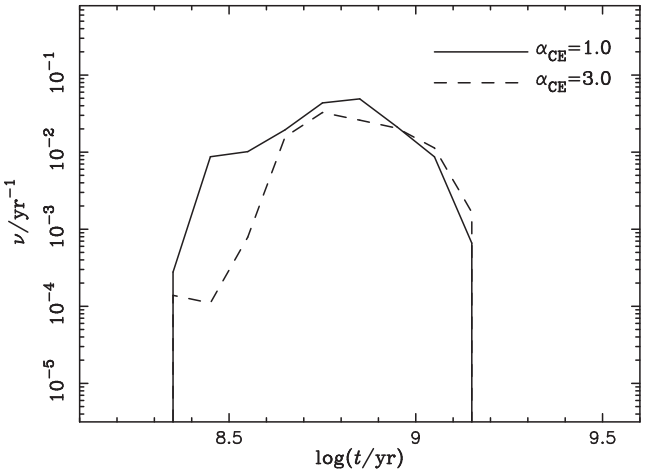

Figure 17. The evolution of the birth rates of SNe Ia for a single starburst of 10^{11} $M_\odot$. The solid and dashed curves show the cases with $\alpha_{CE} = 1.0$ and $\alpha_{CE} = 3.0$, respectively.

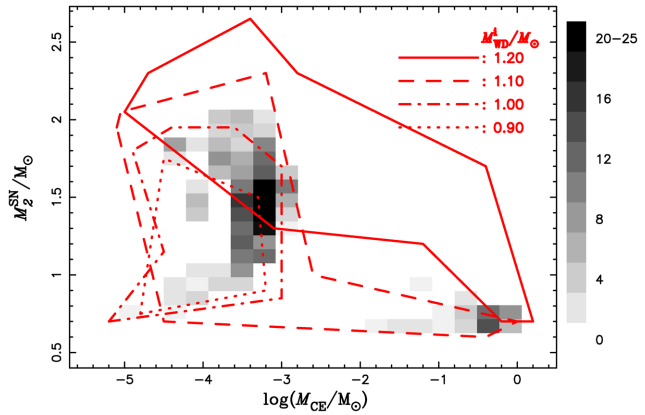

Figure 18. The distribution of the CE mass and the companion mass when $M_{WD} = 1.378\,M_\odot$, and the contour in the (M_{CE}–M_2^{SN}) plane for different initial WD masses. Here, we only show the case of $\alpha_{CE} = 1.0$ since the contours for the case of $\alpha_{CE} = 3.0$ are very similar.

slightly shorter time delays compared to the OTW model as the initial companion can be more massive.

5.2 The CE mass at the time of the SN explosion

Fig. 7 shows that some SNe Ia can explode in the CEW phase, i.e. there is still some material in the CE when $M_{WD} = 1.378\,M_\odot$, which could affect the observational properties of SNe Ia. This is the most significant difference between the CEW and the OTW model. Fig. 18 shows the distribution of the CE mass and the companion mass when $M_{WD} = 1.378\,M_\odot$ and the contour of the CE mass and the companion mass in a $M_2^{SN}-\log(M_{CE})$ plane. Here, we only show the case of $\alpha_{CE} = 1.0$ since the case of $\alpha_{CE} = 3.0$ is similar. Roughly 1.2–14.2 per cent of all SNe Ia explode in the CEW phase, which depends on the value of α_{CE}. The percentage for which SNe Ia explode in the CEW phase in the CEW model is slightly larger than the one for which SNe Ia explode in the OTW phase in the OTW model (Meng, Yang & Geng 2010; Meng & Yang 2011b). The CE mass ranges from 10^{-5} to $\sim$1 $M_\odot$. For most cases, the CE mass lies between a few 10^{-4} and a few 10^{-3} $M_\odot$. It may be difficult to detect such hydrogen-rich material directly; however, such low-mass CEs might leave footprints in the high-velocity features in the spectrum of SNe Ia (Mazzali et al. 2005a,b).

In some cases, the CE mass can be larger than 0.1 $M_\odot$, even as large as 1 $M_\odot$. If the SNe Ia occurs in such situations, hydrogen lines should easily be detectable in the early spectra of some SNe Ia. While such strong hydrogen lines were indeed discovered in some SNe Ia, such as SN 2002ic (Hamuy et al. 2003), this is not consistent with observations of most SNe Ia. This may require a time delay between the moment when $M_{WD} = 1.378\,M_\odot$ and the SN explosion; this time needs to be long enough so that the CE material can be lost. Based on the CE mass and the mass-reduction rate of the CE, we estimate that at least a few 10^5 yr is needed for such a delay time. Obviously, a simmering phase, lasting $\sim 10^3$ yr, of the WD before the SN explosion does not produce such a delay time (Piro & Chang P. 2008; Chen, Han & Meng 2014). A possible suggested mechanism is provided by the spin-up/spin-down model (Justham 2011; Di Stefano & Kilic 2012), where the WD is spun up by accretion. If the resulting WD's rotation velocity is sufficiently large, the WD may not explode as an SN Ia even when its mass exceeds 1.378 $M_\odot$. Hence to explode, a spin-down phase of the WD is required. During the spin-down phase, the companion may lose almost all of its hydrogen-rich envelope and become a very faint object. Such a mechanism may explain the lack of hydrogen lines in the late-time spectrum of SNe Ia predicted by the interaction between the SN ejecta and a hydrogen-rich companion, and why no surviving companion has been found, e.g. in the SN remnant SNR 0509−67.5 (Justham 2011; Di Stefano & Kilic 2012). However, from a purely theoretical point of view, it is completely unclear how long the spin-down time-scale is (Di Stefano, Voss & Claeys 2011). Recently, based on the observational fact that CSM exists around some SNe Ia, Meng & Podsiadlowski (2013) provided a constraint on the spin-down time-scale using a semi-empirical method; they found that the spin-down time-scale should be shorter than a few 10^7 yr, otherwise it would be impossible to detect the signature of the CSM. Such a time-scale is long enough to erase most of the possible observational signatures predicted by the SD model, but short enough that it does not affect the delay time of SN explosions[9] since the formation of the primordial system. 10^5 yr is needed for our CEW model to fulfil the constraint in Meng & Podsiadlowski (2013). Because of the possibility of relatively massive initial companions (in the top right corner in Fig. 7), the delay time for SNe Ia exploding in the CE phase with $M_{CE} > 0.1\,M_\odot$ ranges from 240 to 330 Myr. We estimate that no more than 1.7 in 100 SNe Ia belong to this subclass. Those SNe Ia exploding in massive CEs may contribute to 2002ic-like SNe Ia since their birth rate and delay time is consistent with those estimated from observations, and a strong hydrogen line is expected from the interaction between the SN ejecta and a massive CE (Aldering et al. 2006).

In Fig. 18, there is a gap in the distribution of M_{CE}, which is mainly caused by the different evolutionary stages of the companion stars at the onset of RLOF which sets the mass-transfer time-scale. Generally, the mass-transfer time-scale for companion stars more massive than $\sim 2\,M_\odot$ does not vary monotonically with evolutionary stage from the ZAMS to the bottom of the RGB (Podsiadlowski et al. 2002). Consequently, the critical mass ratio for dynamically unstable mass transfer also does not vary monotonically with the evolutionary stage, which itself is determined by the orbital period of the system at the beginning of RLOF (Ge et al. 2015). Generally,

[9] The delay time is the time that has elapsed between the formation of the primordial binary and the SN event.

Downloaded from https://academic.oup.com/mnras/article-abstract/469/4/4763/3820926
by Said Business School user
on 16 February 2018

for a given binary system, a longer mass-transfer time-scale means a lower average mass-transfer rate. If RLOF begins when the companion crosses the HG, the exact evolutionary stage that gives the longest mass-transfer time-scale depends on the initial companion mass. Systems with the longest mass-transfer time-scale are more likely to be found in the SSS phase when $M_{\rm WD} = 1.378\,{\rm M}_{\odot}$ rather than in the CEW phase, although systems with the same initial WD and companion masses but with shorter or longer orbital periods may explode in the CEW phase or experience a delayed dynamical instability (see panel 7 in Fig. 7).

For those with longer orbital periods, the mass-transfer time-scale sharply decreases with orbital period, which results in a very high mass-transfer rate; then the CE mass may be larger than $0.1\,{\rm M}_{\odot}$ at the time of the SN explosion, an example of which is shown in Fig. 4. In addition, for very high mass-transfer rates, the companion will lose its outer envelope quickly. With the loss of the companion's envelope, the hydrogen fraction of the transferred material decreases, which results in a higher critical accretion rate and hence a higher mass-growth rate of the CO WD (see equation 12 and panels 2 and 3 in Fig. 4). So, the time from the onset of RLOF to the moment of the SN explosion is shortened; this also contributes to the population of SNe with massive CEs as the time-scale for losing the CE is also shortened. However, such cases only occur for systems with initial WD masses $\geq 1.1\,{\rm M}_{\odot}$ and relatively massive companions.

For those with shorter initial orbital periods, the mass-transfer time-scale may become so short that the systems experience a delayed dynamical instability if the mass ratio of the donor star to the WD is sufficiently high. Such systems may eventually merge and hence not contribute to the SN Ia population. If the mass ratio is not very high, the mass-transfer time-scale of the systems with a shorter initial orbital period will become shorter, but not much shorter than the longest mass-transfer time-scale. This implies a relatively higher, but not much higher mass-transfer rate. So, a massive CE is difficult to maintain for very high mass-loss rates from the surface of the CE. Even for the cases almost experiencing a delayed dynamical instability, the massive CE can also not be maintained for a long time (see also Fig. 6). At the moment when $M_{\rm WD} = 1.378\,{\rm M}_{\odot}$, the mass-transfer rate of these systems is generally slightly larger than the critical accretion rate, which means that the CE cannot be very massive, e.g. $\leq 10^{-3}\,{\rm M}_{\odot}$. Additionally, the failure to maintain a massive CE at the time of the SN explosion is also partly caused by the relatively longer mass-growth time-scales of the WDs, even for systems with the same initial WD mass, due to the unchanged hydrogen mass fraction (see the different explosion times in Figs 4 and 6). SNe Ia that explode in a low-mass CE predominantly occur for systems with initial WD masses $\leq 1.0\,{\rm M}_{\odot}$, where the mass-growth time-scale of the WDs is too long to maintain a very massive CE at the time of the explosion. Therefore, if a system explodes in the CEW phase, the CE tends to have a mass of either $\leq 10^{-3}\,{\rm M}_{\odot}$ or $\geq 0.1\,{\rm M}_{\odot}$, which leads to the gap in the distribution of $M_{\rm CE}$. Moreover, as clearly shown by the red and green points at the bottom of panel (7) in Fig. 9, the companions for those WDs exploding in a high-mass CE are less massive than the ones exploding in a low-mass CE.

6 DISCUSSION

6.1 Uncertainties in the CEW model

In this paper, we constructed a new SD model in which a CE forms around the binary when the mass-transfer rate exceeds the critical accretion rate. Material in the CE is lost from the surface of the CE instead from the WD surface in the OTW model. Many of the results in the CEW model are similar to those in the OTW model, such as the evolution of binary parameters, while the parameter space leading to SNe Ia and the birth rate of SNe Ia in the CEW model are somewhat larger than in the OTW model. However, the CEW model as presented in this paper is still very simple at present with numerous uncertainties in the detailed modelling. In the following, we discuss some of the main uncertainties in our new CEW models one by one.

In the CEW model, one of the main uncertainties arises from the assumed CE density. In this paper, we simply assumed that the CE is spherical and used an average density to replace the density at the boundary of the inner and the outer part of the CE. The density ρ directly affects the effective turbulent viscosity (equation 3), and hence the angular-momentum loss from the binary system, the frictional luminosity and consequently the mass loss from the system. To test the effect of varying the CE density on the final parameter contours leading to SNe Ia, we arbitrarily multiplied the density in equation (6) by factors of 0.1 and 10, respectively, and recalculated the contour leading to SNe Ia for $M^{\rm i}_{\rm WD} = 1.1\,{\rm M}_{\odot}$. Fig. 19 provides an example to show how the average density affects the binary evolution. The figures show that, as one might expect, a higher average density results in a higher frictional luminosity and a higher mass-transfer rate, and hence leads to a more massive CE. If the average density is high enough, i.e. the density is increased by a factor of 20 or larger, the system will experience a dynamical instability and the system will eventually merge. The critical density factor is system dependent. For example, for the system with $(M^{\rm i}_{\rm WD}/{\rm M}_{\odot}, M^{\rm i}_{2}/{\rm M}_{\odot}, \log(P^{\rm i}/{\rm d})) = (0.8, 2.2, 0.4)$, the critical density factor is 250 due to a much less massive CE. In addition, the evolutionary track of the companion in the HR diagram is significantly affected by the frictional density, as is the period. Fig. 20 shows how the density factor affects the final state of the binary system when $M_{\rm WD} = 1.378\,{\rm M}_{\odot}$: the companion mass, orbital period and the mass-transfer time-scale decrease, while the CE mass increases with the density factor. This is a direct consequence of the higher frictional luminosity as this leads to a larger loss of orbital angular momentum due to the friction between the binary system and the CE; this leads to a higher mass-transfer rate and a more massive CE. At the same time, the companion will lose more material and becomes less massive, i.e. may be as small as $0.5\,{\rm M}_{\odot}$ at the time when $M_{\rm WD} = 1.378\,{\rm M}_{\odot}$. Due to the relatively small radius for the shorter orbital period, the companion also has a low luminosity, i.e. is dimmer than $1\,{\rm L}_{\odot}$. The relatively short mass-transfer time-scale for a large density factor here is a direct consequence of equation (12). A high density factor results in a higher mass-transfer rate, and the companion will lose its outer envelope more quickly. With the loss of the companion's envelope, the hydrogen fraction of the transferred material decreases; this leads to a higher critical accretion rate and a higher mass-growth rate of the CO WD (see panels 2 and 3 in Figs 4 and 19) and a shorter overall mass-transfer time-scale. The influence of high density on the companion could provide some clues in searches for surviving companions in SN remnants, e.g. a dim MS star with a relatively low surface hydrogen fraction.

However, we find that the contours leading to SNe Ia in the $(\log P_{\rm i}, M^{\rm i}_{2})$ planes for different average densities is more or less the same as that shown in Fig. 8, irrespective of the density factor, except that more SNe Ia explode in the CE phase for a higher assumed CE density. As shown in Fig. 20, the higher the frictional density, the more massive the CE, making it more likely that the SN explodes in the CE phase. As far as the contours resulting in

Downloaded from https://academic.oup.com/mnras/article-abstract/469/4/4763/3820926
by Said Business School user
on 16 February 2018

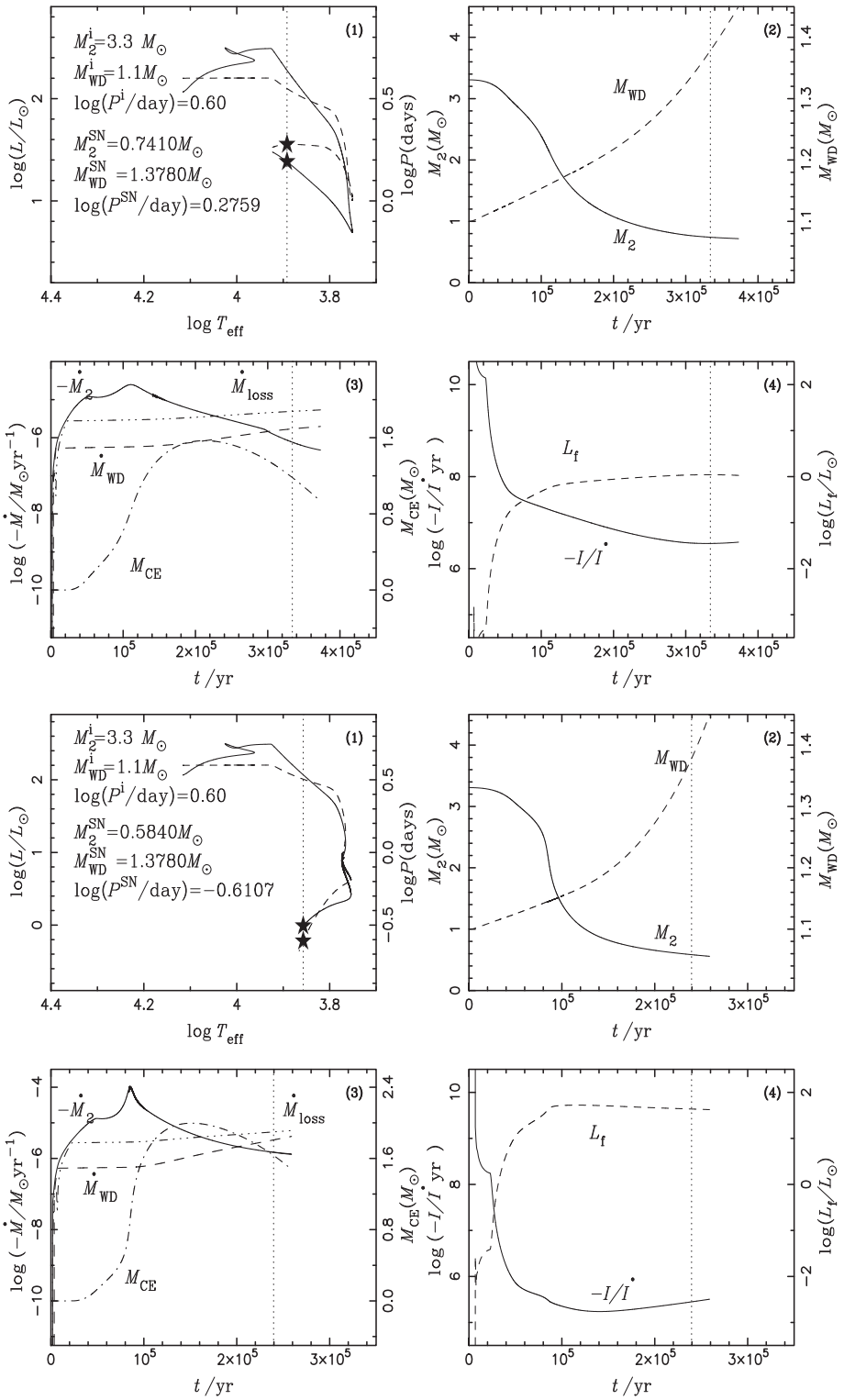

Figure 19. Similar to Fig. 4 but for a different average CE density. The average density from equation (6) is arbitrarily multiplied by a factor of 0.1 (top four panels) and 10 (bottom four panels).

SNe Ia is concerned, only the upper boundary, which is determined by systems that experience a delayed dynamical instability, would be significantly affected by the frictional density. For a given system, the higher the frictional density, the more likely the system experiences a delayed dynamical instability, moving the upper boundary downwards. However, as discussed above, although this is model dependent, only when the density factor is larger than $\simeq 20$ would systems that avoid the merging fate in our standard model experience a delayed dynamical instability. Therefore, within the density range tested here, the upper boundaries of the contours are almost unaffected by the density factor. The left and right boundaries are determined by the radius of stars on the ZAMS, or at the end of

Downloaded from https://academic.oup.com/mnras/article-abstract/469/4/4763/3820926
by Said Business School user
on 16 February 2018

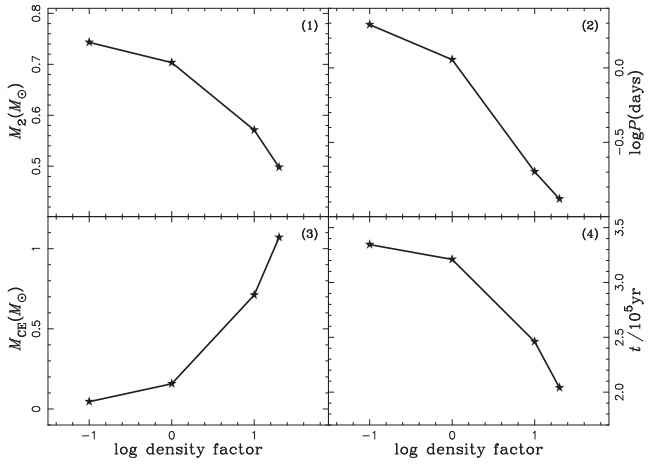

Figure 20. The companion mass, orbital period, CE mass and mass-transfer time-scale (from the onset of RLOF to the SN explosion) when $M_{WD} = 1.378\,M_\odot$ as a function of the density factor, where the initial parameter of the model is $[M^i_{WD}/M_\odot, M^i_2/M_\odot, \log(P^i/d)] = (1.1, 3.3, 0.6)$.

the HG, which are completely unaffected by the density factor. The lower boundary is constrained by the condition that the secondaries are massive enough to increase the WD mass to $1.378\,M_\odot$. This condition is very weakly dependent on the frictional density factor as discussed above for a system with $(M^i_{WD}/M_\odot, M^i_2/M_\odot, \log(P^i/d)) = (0.8, 2.2, 0.4)$.

Another key uncertainty arises from the adopted mass-loss rate from the surface of the CE, which determines the mass left in the CE; there is no well-established prescription for mass loss from a CE (cf. Schröder & Cuntz 2007). Here, we again arbitrarily multiply the mass-loss rate in equation (8) by a factor of 0.1 or 10. Fig. 21 shows an example of how the mass-loss rate affects the binary evolution and the final state of the binary system. Figs 4 and 21 show that the wind mass-loss rate does not affect the binary evolution as significantly as the density does, while it may influence the CE mass considerably. There is a clear trend that, for a lower wind mass-loss rate, WDs tend to reach $1.378\,M_\odot$ during the CE phase, while WDs are more likely to explode in the SSS or RN phase for the higher mass-loss rates. In other words, for a higher mass-loss rate, it becomes more difficult to maintain the CE while it is relative easy to obtain a more massive CE for a lower mass-loss rate. In fact, when the wind enhancement factor is larger than 10, the effect of the CEW on the evolution of the binary is rather minor, and the evolution is very similar to that of the OTW. However, the WD may gradually increase its mass to $1.378\,M_\odot$ for any mass-loss rate. Fig. 22 shows how the wind enhancement factor affects the final state of the binary system. The wind mass-loss rate only has a minor effect on the SN formation rate when the wind mass-loss rate is sufficiently low (the wind factor is lower than 0.1), although a lower wind factor favours the existence of the CE. This directly follows from equation (7), i.e. $\dot{M}_{CE} = |\dot{M}_2| - \dot{M}_{WD} - \dot{M}_{wind} \simeq |\dot{M}_2| - \dot{M}_{WD}$ when the wind mass-loss rate is much lower than $\dot{M}_2$ and $\dot{M}_{WD}$ and can therefore be neglected. Thus, if the wind factor is low enough, the evolution of the CE no longer depends on the mass-loss rate.

Fig. 23 presents a map for SNe Ia and mergers in the density – wind factor plane; the boundary between SNe Ia and mergers is also shown in the figure. The figure illustrates that the boundary is system dependent, especially for the density factor. However, for a rather large parameter region, binary systems may avoid the fate of merging, demonstrating that the CEW model is rather robust.

The factor α in equation (1) is also an important factor which directly affects the orbital angular-momentum loss and the frictional luminosity. Its influence on the binary evolution is quite similar to the changes in the frictional density as already discussed above.

In this paper, we assumed that all the potential energy sources, i.e. from nuclear burning, the secondary's luminosity and the frictional luminosity are contributing to driving the wind mass loss. A small part of that energy will be required to drive the expansion of the CE itself, which could moderately decrease the expected mass loss. However, as we discussed above, there is a rather large parameter range for which the assumptions about the wind do not affect whether a binary system explodes as a SN Ia or not. Therefore, this effect is unlikely to change the main conclusions of this paper.

We also assumed that the presence of an envelope changes the helium flash at the bottom of the hydrogen-burning shell like in a TPAGB star. On the other hand, if the CE is not massive enough and the helium flash is strong enough, the CE might be destroyed. We plan to study the conditions for which the destruction of the CE can be prevented in the future.

Finally, for the CEW model it is still unclear what the system actually would look like during the CE phase; this will depend on the CE mass, the nuclear luminosity for hydrogen and helium burning and the percentage of the total energy used to drive the mass loss from the surface of the CE. In general, we would expect an RG-like object with a high luminosity. We will address this issue in the future following the approach developed previously in Podsiadlowski, Joss & Rappaport (1990).

In summary, our CEW model as it stands now is still very simple, but most of our assumptions are rather conservative. We therefore consider the results in this paper only as the first step and we intend to refine the model in the future.

6.2 The differences between the CEW model and the OTW model

The physical assumptions in the CEW model and the OTW model are quite different, which should lead to several testable differences between the two models.

(1) The CEW model does not directly depend on metallicity; hence, it allows SNe Ia to occur in any environment irrespective of metallicity and redshift. Thus, the discovery of some SNe Ia at high redshifts and/or in a low-metallicity environment are easily explained in the CEW model. The lack of a low-metallicity threshold for SNe Ia relative to SNe II is also a natural result in the CEW model.

(2) When $|\dot{M}_2|$ exceeds $\dot{M}_{cr}$, the hydrogen-rich material burns stably on the WD at a rate of $\dot{M}_{cr}$, while the unprocessed material forms the CE. At the same time, some CE material may leave the system from the surface of the CE. This treatment leads to two significant differences between the CEW model and the OTW model. One is that the mass-growth rate of the WD in the CEW model is larger than that in the OTW model, which results in a larger initial parameter space for SNe Ia and a lower minimum WD mass, and hence a higher birth rate. The other is the wind velocity. In the CEW model, the unprocessed material leaves the system from the surface of the CE instead of the surface of the WD, resulting in a much lower wind velocity than in the OTW model, i.e. most likely less than 200 $km\,s^{-1}$, probably lower than 50 $km\,s^{-1}$. Our model is therefore compatible with the dynamics of the forward shock and the X-ray emission from the shocked ejecta in SN Ia

Downloaded from https://academic.oup.com/mnras/article-abstract/469/4/4763/3820926
by Said Business School user
on 16 February 2018

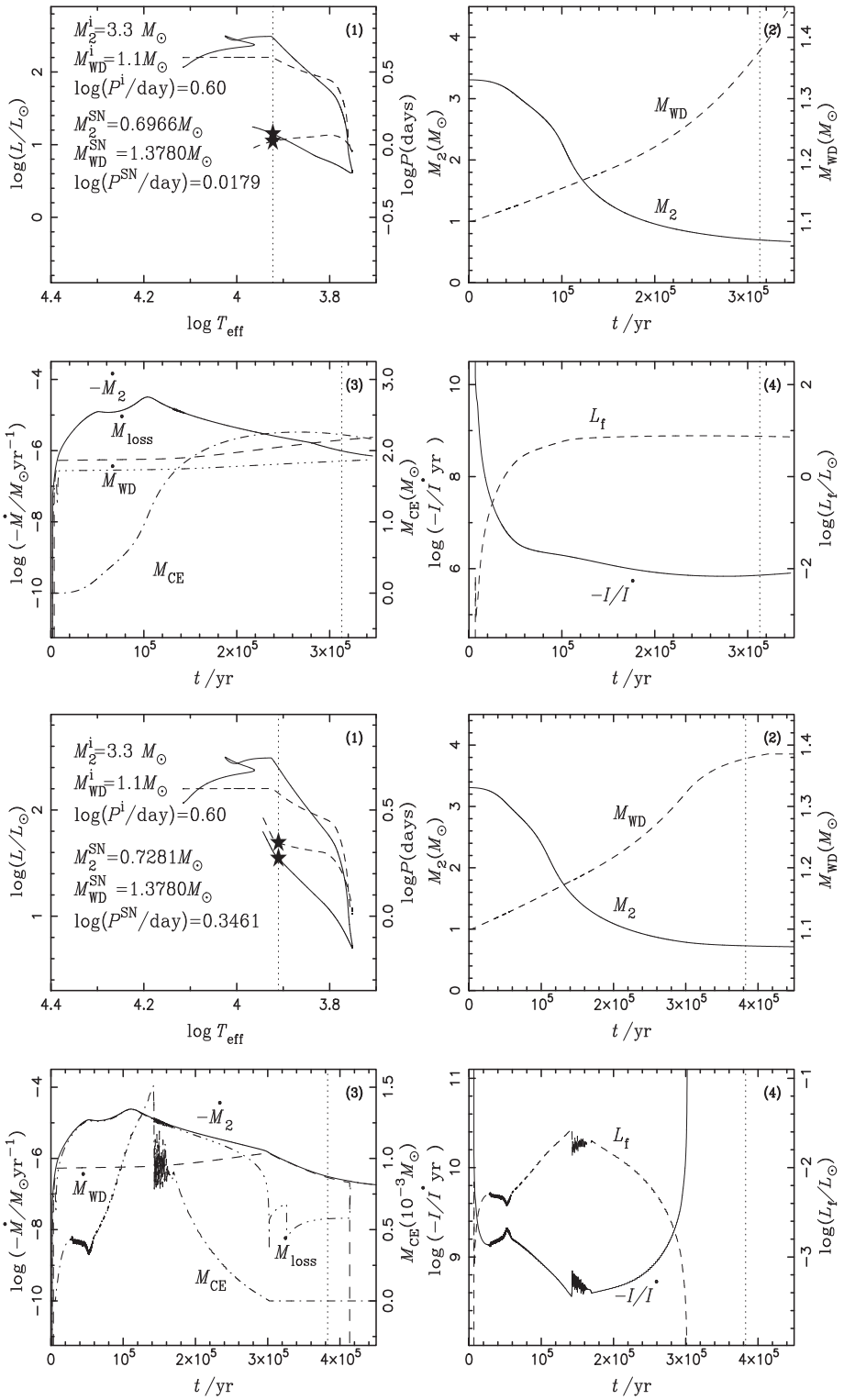

Figure 21. Similar to Fig. 4 but for a different mass-loss rate. The mass-loss rate from equation (8) is arbitrarily multiplied by a factor of 0.1 (top four panels) or 10 (bottom four panels).

remnants examined by Badenes et al. (2007). Even the properties of RCW 86, where the wind cavity with a diameter of ∼30 pc contains 1.6 $M_\odot$ of material ejected from the progenitor system (Broersen et al. 2014), may be explained by our model since a low-density cavity around some SNe Ia could also be expected for some cases in our model grid (see Fig. 15).

(3) When the hydrogen-rich material is stably burning on the surface of the WD, soft X-ray emission is expected from the mass-accreting WD and the system will appear as an SSS (van den Heuvel 1992), while no strong X-ray emission is expected from the DD scenario until just before the SN Ia explosion. This provides a potential method for distinguishing between SD and DD models.

Downloaded from https://academic.oup.com/mnras/article-abstract/469/4/4763/3820926
by Said Business School user
on 16 February 2018

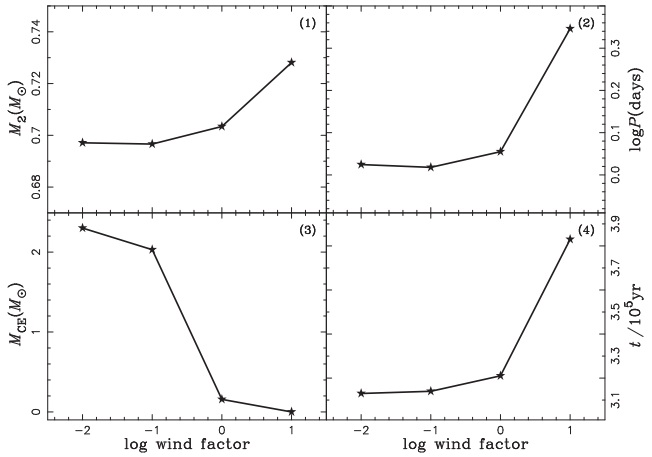

Figure 22. The companion mass, orbital period, CE mass and mass-transfer time-scale (from the onset of RLOF to the SN explosion) when $M_{WD} = 1.378\,M_\odot$ as a function of the wind factor, where the initial parameter of the model is ($M^i_{WD}/M_\odot$, $M^i_2/M_\odot$, $\log(P^i/d)$)= (1.1, 3.3, 0.6).

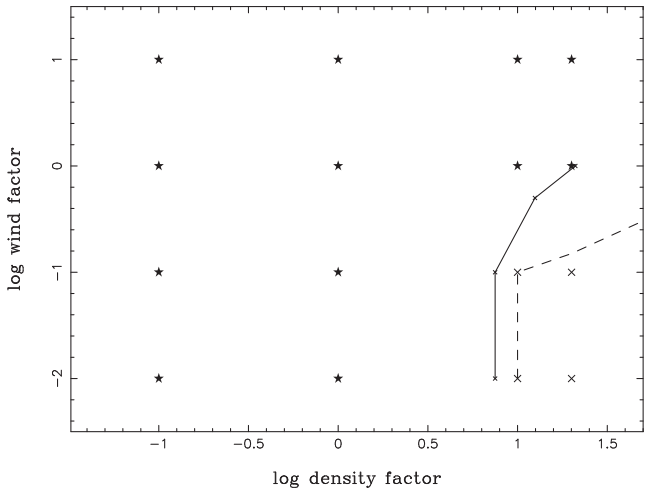

Figure 23. The map for SNe Ia and mergers in the density–wind factor plane [for a representative system with initial parameters of ($M^i_{WD}/M_\odot$, $M^i_2/M_\odot$, $\log(P^i/d)$) = (1.1, 3.3, 0.6) and (0.8, 2.2, 0.4), respectively]. Stars represent systems that explode as SNe Ia, while crosses indicate systems that merge. The solid and dashed curves show the boundary between SNe Ia and mergers obtained from the systems of (1.1, 3.3, 0.6) and (0.8, 2.2, 0.4), respectively.

However, the number of the SSSs in elliptical and spiral galaxies is much smaller than that predicted from the standard SD model (Di Stefano 2010; Gilfanov & Bogdán 2010). The predicted number of SSSs from the SD model in these studies is based on the assumption that all the accreting WDs are in the SSS phase that lasts for about 2 Myr before the SN Ia explosion. This assumption is rather simple and may overestimate the duration of the SSS phase by a factor of 10 (see panel 3 in Figs 2 and 4). According to the OTW model, in which the OTW may absorb the soft X-rays, the duration of the SSS phase is much shorter; Hachisu, Kato & Nomoto (2010) and Meng & Yang (2011b) were able to reproduce the observed SSS number in elliptical and spiral galaxies, i.e. only a small fraction of mass-accreting WDs resulting in SNe Ia contributes to the supersoft X-ray flux of a galaxy. In the CEW model, because of the existence of the CE, X-rays would be completely absorbed by the CE or the material lost from the CE surface. The duration of the SSS phase

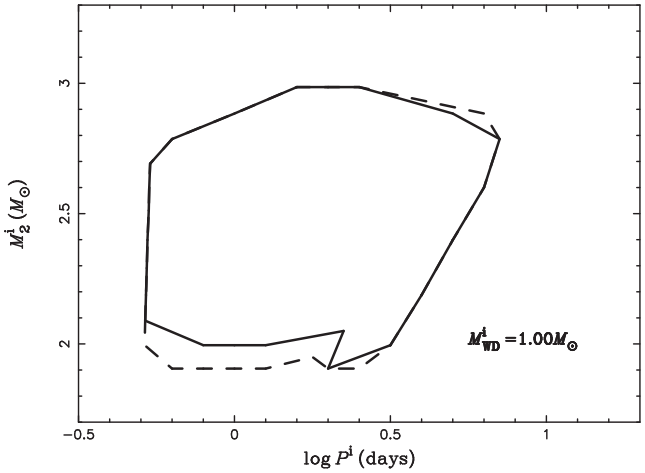

Figure 24. Contours leading to SNe Ia in the secondary mass–orbital period plane for $M^i_{WD} = 1.0\,M_\odot$. The solid curve is for η_{He} in Kato & Hachisu (2004) and the dashed curve is for η_{He} arbitrarily increased by 50 per cent, i.e. $\eta'_{He} = \min(1, 1.5\eta_{He})$.

in the CEW model would be even shorter than in the OTW model since, even when $|\dot{M}_2|$ is smaller than $\dot{M}_{cr}$, a CE can still exist (see the panel 3 in Fig. 4). So, the CEW model is likely to be consistent with the observations of Gilfanov & Bogdán (2010) and Di Stefano (2010) (also see the discussion about the SSS phase in Maoz et al. 2014).

(4) The OTW model may explain the properties of some RNe that have been suggested as potential progenitors of SNe Ia (Hachisu & Kato 2005, 2006a,b; Hachisu et al. 2007); this also applies to the CEW model as the CEW model reduces to the OTW model when there is no CE.

(5) The efficiency of the accretion of hydrogen on massive WDs at a high rate over many cycles is still controversial; this affects the conditions for which SNe Ia can occur. For example, Idan, Shaviv & Shaviv (2013) recently concluded that the accumulated helium under the hydrogen-burning shell is completely lost in a strong helium flash, which, taken at face value, would make SNe Ia impossible. On the other hand, Newsham, Starrfield & Timmes (2014) conclude that a WD may continue to increase its mass towards the Chandrasekha limit. The helium accumulation efficiency, η_{He}, used here is usually smaller than 1 even when hydrogen burns at a rate of $\dot{M}_{cr}$. Fortunately, although it is not clear how the WD adjusts to alternating helium flashes and stable hydrogen shell burning in the OTW model, this issue probably does not arise in the CEW model. In addition, η_{He} could be larger than derived by Kato & Hachisu (2004) if the effect of H shell burning has been accounted for, since the nuclear energy produced via H-burning keeps the underlying He buffer hotter, resulting in weaker and more frequent He flashes (Cassisi, Iben & Tornambè 1998). Especially, Hillman et al. (2016) recently found that, although a significant fraction of the material accumulated prior to the flash is lost during the first few helium shell flashes, the fraction decreases with repeated helium shell flashes and eventually no mass is lost at all during subsequent flashes. In addition, the helium shell flash in a rapidly rotating WD due to accretion will become more stable than in the corresponding non-rotating WD (Yoon & Langer 2004a,b). We tested the effect of the accumulation efficiency of helium flashes on the parameter space leading to SNe Ia by increasing η_{He} by 50 per cent rather arbitrarily (but keeping the maximum value of η_{He} at 1). Fig. 24 shows a comparison of the contours leading to SNe Ia for different

Downloaded from https://academic.oup.com/mnras/article-abstract/469/4/4763/3820926
by Said Business School user
on 16 February 2018

values of $\eta_{\rm He}$. The figure shows that a higher $\eta_{\rm He}$ moves the lower boundary to a lower value while the other boundaries are almost unaffected by a change of $\eta_{\rm He}$. The reason is that $\eta_{\rm He}$ only plays a role in phases of stable burning or weak hydrogen flashes (see Fig. 7). In addition, for a lower initial WD mass (<0.9 $M_\odot$), most SNe Ia explode in the SSS or RN phase, where $\eta_{\rm He}$ may play a more important role, i.e. a high $\eta_{\rm He}$ results in a larger parameter space for SNe Ia. So, a higher $\eta_{\rm He}$ could lead to a relatively higher birth rate of SNe Ia and produce SNe Ia in an older population.

(6) As far as the possible appearance of a WD in the OTW phase is concerned, Nomoto et al. (2007) suggested that the system might look like an undersized OB star, i.e. with an effective temperature of 31 600–10 000 K, but with a size of only a few $R_\odot$, limited by the WD's Roche lobe radius. However, no such rapidly accreting blue white dwarf has been found in searches in the Large Magellanic Cloud (Lepo & van Kerkwijk 2013a). Alternatively such systems might look like Wolf–Rayet stars or WD planetary nebulae (see also Lepo & van Kerkwijk 2013a; Nielsen et al. 2013; Wheeler & Pooley 2013). It is worth emphasizing that, for most cases, when the mass-transfer rate is very high, i.e. higher than 10^{-5} $M_\odot$ yr^{-1} (see Han & Podsiadlowski 2004 and Meng et al. 2009a), the OTW must carry away a large amount of dynamic energy that almost equals the nuclear burning energy. So, during the OTW phase, the WD must be dimmer. In the CEW model, we suggest that the system resembles a TPAGB star during the CE phase. If the system loses the envelope before the SN, it could look like a post-AGB star. After the CE phase, the accreted hydrogen-rich material burns stably on the surface of the WD, and the system may show the properties of a SSS, which is a powerful source of ionizing ultraviolet emission. Such ultraviolet photons may ionize helium in the CSM or interstellar medium, and then emission in the recombination lines of He II could be expected. Interestingly, searching for the recombination radiation of He II in passively evolving galaxies, Johansson et al. (2014) found that the strength of the observed He II λ4686 nebular emission is consistent with the post-AGB stars being the sole ionizing source. In addition, during the CE phase, if the envelope is massive enough, a high luminosity, i.e. even higher than the Eddington luminosity of the WD, and a variable high mass-loss rate for helium flashes might be expected. LMC N66 in the Large Magellanic Cloud could be an interesting candidate: it consists of a WD primary and a non-degenerate system in the centre and experiences huge mass loss with a highly variable mass-loss rate (Lepo & van Kerkwijk 2013b). In any case, it is still unclear how to distinguish these from real TPAGB stars, and a detailed study on the appearance of the binary system for our CEW model is still required. We have started such an investigation and will report the results in a future publication.

(7) One question that has been raised for a long time since Hachisu et al. (1996, 1999b) is whether the OTW model requires too much fine-tuning (e.g. Piersanti et al. 2000; Shen & Bildsten 2007; Woosley & Kasen 2011). In contrast, as discussed in Section 6.1, our CEW model is rather robust and may work within a very large parameter range, probably requiring much less fine-tuning (see Fig. 23).

7 SUMMARY AND CONCLUSION

We have constructed a new SD model for SNe Ia in which a common envelope forms when the mass-transfer rate on to the WD exceeds a critical accretion rate instead of an OTW. Based on the CEW model, we investigated in detail the WD+MS channel using detailed binary evolution calculations. The initial parameters for SNe Ia in the ($\log P^{\rm i}$, $M_2^{\rm i}$) plane were obtained and then used to study the evolution of the birth rate of SNe Ia by a BPS method. In the following, we summarize the main results.

(1) The parameter space obtained from our new CEW model is slightly larger than that in the OTW model, i.e. it allows a higher initial companion mass and longer initial orbital period. The minimum WD mass leading to SNe Ia is 0.65 $M_\odot$, slightly lower than in the OTW model.

(2) We also presented the final parameters of the binary systems and the companion properties at the time of the SN explosion, which may be helpful for identifying progenitor systems or search for surviving companions in SN remnants. Several observed SSSs and RN systems lie in the parameter regions for SNe Ia, making them ideal candidates for SN Ia progenitors. The properties of Tycho G, the suggested surviving companion of Tycho's SN, is also consistent with our results.

(3) Before the SN Ia explosion, the system may lose as much as 2.5 $M_\odot$ of hydrogen-rich material, where there is a trend that, the more mass is lost, the closer the maximum distance this material may reach. For some SNe Ia, the material may be less than 0.2 $M_\odot$, spread over a very large region, possibly extending to more than 300 pc. The environment around these SNe Ia could be very clean and it would be very difficult to detect a signature of this CSM around such SNe Ia.

(4) A significant fraction of SNe Ia may explode in the CE phase with a CE mass from a few 10^{-4} $M_\odot$ to a few 10^{-3} $M_\odot$; these might be essential for explaining the high-velocity Ca features seen in the spectrum of SNe Ia (Mazzali et al. 2005a,b).

(5) For a single starburst, most SNe Ia occur between 0.25 Gyr and 2 Gyr, while the Galactic birth rate of the SNe Ia from our CEW model is $(0.89–1.20)\times10^{-3}$ yr^{-1}, which is higher than in the OTW model by about ∼30 per cent.

(6) We examined the uncertainties of our model caused by uncertainties in the modelling parameters and found that the model is very robust within a very large parameter range.

(7) We discussed the differences between the CEW and the OTW model. Our model avoids several of the shortcomings of the OTW model but also shares the merits of the OTW model. Especially, our model does not depend on metallicity, and SNe Ia may occur in low-metallicity and/or high-redshift environments. In addition, the typical outflow velocity should be much lower than in the OTW model since the material is lost from the CE surface instead of the WD surface in the OTW model.

(8) The accumulation efficiency for helium flashes could be a very important factor in determining the parameter space that leads to a successful SN Ia, i.e. a higher $\eta_{\rm He}$ than in Kato & Hachisu (2004) may extend the allowed range of companion masses to a lower initial mass, resulting in a higher birth rate and a possibly longer delay time.

(9) Our model may naturally explain the birth rate and delay time of 2002ic-like SNe Ia.

ACKNOWLEDGEMENTS

We are grateful to the anonymous referee for his/her constructive comments that helped to improve the manuscript greatly. We thank Professor Zhanwen Han for his helpful comments on the manuscript. This work was partly supported by Natural Science Foundation of China (Grant Nos. 11473063, 11522327), CAS (No. KJZD-EW-M06-01), CAS 'Light of West China' Program and Key Laboratory for the Structure and Evolution of Celestial Objects, Chinese Academy of Sciences.

Downloaded from https://academic.oup.com/mnras/article-abstract/469/4/4763/3820926
by Said Business School user
on 16 February 2018

REFERENCES

Aldering G. et al., 2006, ApJ, 650, 510
Alexander D. R., Ferguson J. W., 1994, ApJ, 437, 879
Arnett W. D., 1982, ApJ, 253, 785
Badenes C., Hughes J. P., Bravo E., Langer N., 2007, ApJ, 662, 472
Bedin L. R., Ruiz-Lapuente P., González Hernández J. I., Canal R., Filippenko A. V., Mendez J., 2014, MNRAS, 439, 354
Blondin S., Prieto J. L., Patat F., Challis P., Hicken M., Kirshner R. P., Matheson T., Modjaz M., 2009, ApJ, 693, 207
Borkowski K. J., Hendrick S. P., Reynolds S. P., 2006, ApJ, 652, 1259
Borkowski K. J., Blondin J. M., Reynolds S. P., 2009, ApJ, 699, L64
Branch D., 2004, Nature, 431, 1044
Branch D., Livio M., Yungelson L. R., Boffi F. R., Baron E., 1995, PASP, 107, 1019
Broersen S., Chiotellis A., Vink J., Bamba A., 2014, MNRAS, 441, 3040
Brown P. J., 2014, ApJ, 796, L18
Cao Y. et al., 2015, Nature, 521, 328
Cao Y., Kulkarni S. R., Gal-Yam A., Papadogiannakis S., Nugent P. E., Masci F. J., Bue B. D., 2016, ApJ, 832, 86
Cappellaro E., Turatto M., 1997, in Ruiz-Lapuente P., Cannal R., Isern J., eds, Thermonuclear Supernovae. Kluwer, Dordrecht, p. 77
Cassisi S., Iben I., Jr, Tornambè A., 1998, ApJ, 496, 376
Chen X., Han Z., 2002, MNRAS, 335, 948
Chen X., Han Z., 2003, MNRAS, 341, 662
Chen X., Han Z., 2008, MNRAS, 387, 1416
Chen W., Li X., 2007, ApJ, 658, L51
Chen X., Tout C. A., 2007, Chin. J. Astron. Astrophys., 7, 245
Chen X., Han Z., Tout C. A., 2011, ApJ, 735, L31
Chen X., Han Z., Meng X., 2014, MNRAS, 438, 3358
Chomiuk L., 2013, PASA, 30, 46
Di Stefano R., 2010, ApJ, 712, 728
Di Stefano R., Kilic M., 2012, ApJ, 759, 56
Di Stefano R., Kong A. K. H., 2003, ApJ, 592, 884
Di Stefano R., Voss R., Claeys J. S. W., 2011, ApJ, 738, L1
Dilday B. et al., 2012, Science, 337, 942
Eggleton P. P., 1971, MNRAS, 151, 351
Eggleton P. P., 1972, MNRAS, 156, 361
Eggleton P. P., 1973, MNRAS, 163, 279
Eggleton P. P., Tout C. A., Fitechett M. J., 1989, ApJ, 347, 998
Foley R. J. et al., 2012, ApJ, 744, 38
Frederiksen T. F., Hjorth J., Maund J. R., Rodney S. A., Riess A. G., Dahlen T., Mobasher B., 2012, ApJ, 760, 125
Fuhrmann K., 2005, MNRAS, 359, L35
Galbany L. et al., 2016, A&A, 591, A48
Ge H., Webbink R. F., Chen X., Han Z., 2015, ApJ, 812, 40
Ghavamian P., Raymond J., Smith R. C., Hartigan P., 2001, ApJ, 547, 995
Gilfanov M., Bogdán A., 2010, Nature, 463, 924
Goldberg D., Mazeh T., 1994, A&A, 282, 801
González-Hernández J., Ruiz-lapuente P., Filippenko A., Foley R. J., Gal-Yam A., Simon J. D., 2009, ApJ, 691, 1
Graur O., Zurek D., Shara M. M., Riess A. G., Seitenzahl I. R., Rest A., 2016, ApJ, 819, 31
Greggio L., Renzini A., 1983, A&A, 118, 217
Hachisu I., Kato M., 2000, ApJ, 540, 447
Hachisu I., Kato M., 2001, ApJ, 558, 323
Hachisu I., Kato M., 2003a, ApJ, 588, 1003
Hachisu I., Kato M., 2003b, ApJ, 590, 445
Hachisu I., Kato M., 2005, ApJ, 631, 1094
Hachisu I., Kato M., 2006a, ApJ, 642, L52
Hachisu I., Kato M., 2006b, ApJ, 651, L141
Hachisu I., Kato M., Nomoto K., 1996, ApJ, 470, L97
Hachisu I., Kato M., Nomoto K., Umeda H., 1999a, ApJ, 519, 314
Hachisu I., Kato M., Nomoto K., 1999b, ApJ, 522, 487
Hachisu I., Kato M., Kato T., Matsumoto K., 2000a, ApJ, 528, L97
Hachisu I., Kato M., Kato T., Matsumoto K., Nomoto K., 2000b, ApJ, 534, L189
Hachisu I., Kato M., Schaefer B. E., 2003, ApJ, 584, 1008
Hachisu I., Kato M., Luna G. J. M., 2007, ApJ, 659, L153
Hachisu I., Kato M., Nomoto K., 2008, ApJ, 679, 1390
Hachisu I., Kato M., Nomoto K., 2010, ApJ, 724, L212
Hachisu I., Kato M., Saio H., Nomoto K., 2012, ApJ, 744, 69
Hamuy M. et al., 2003, Nature, 424, 651
Han Z., 2008, ApJ, 677, L109
Han Z., Podsiadlowski Ph., 2004, MNRAS, 350, 1301
Han Z., Podsiadlowski Ph., 2006, MNRAS, 368, 1095
Han Z., Podsiadlowski P., Eggleton P. P., 1994, MNRAS, 270, 121
Han Z., Podsiadlowski P., Eggleton P. P., 1995, MNRAS, 272, 800
Han Z., Tout C. A., Eggleton P. P., 2000, MNRAS, 319, 215
Han Z., Podsiadlowski Ph., Maxted P. F. L., Marsh T. R., Ivanova N., 2002, MNRAS, 336, 449
Helder E. A. et al., 2009, Science, 325, 719
Hillebrandt W., Niemeyer J. C., 2000, ARA&A, 38, 191
Hillman Y., Prialnik D., Kovetz A., Shara M. M., 2016, ApJ, 819, 168
Hjellming M. S., Webbink R. F., 1987, ApJ, 318, 794
Howell D. A., 2011, Nat. Commun., 2E, 350
Howell D. A. et al., 2009, preprint (arXiv:0903.1086)
Hurley J. R., Pols O. R., Tout C. A., 2000, MNRAS, 315, 543
Hurley J. R., Tout C. A., Pols O. R., 2002, MNRAS, 329, 897
Iben I., Tutukov A. V., 1984, ApJS, 54, 335
Idan I., Shaviv N. J., Shaviv G., 2013, MNRAS, 433, 2884
Iglesias C. A., Rogers F. J., 1996, ApJ, 464, 943
Ilkov M., Soker N., 2012, MNRAS, 419, 1695
Ilkov M., Soker N., 2013, MNRAS, 428, 579
Ivanova N. et al., 2013, A&AR, 21, 59
Ivanova N., Justham S., Podsiadlowski Ph., 2015, MNRAS, 447, 2181
Johansson J., Woods T. E., Gilfanov M., Sarzi M., Chen Y.-M., Oh K., 2014, MNRAS, 442, 1079
Jones D. O. et al., 2013, ApJ, 768, L166
Justham S., 2011, ApJ, 730, L34
Kasen D., 2010, ApJ, 708, 1025
Kato M., Hachisu I., 2004, ApJ, 613, L129
Kato M., Hachisu I., 2012, Bull. Astron. Soc. India, 40, 393
Kerzendorf W. E. et al., 2009, ApJ, 701, 1665
Kerzendorf W. E. et al., 2013, ApJ, 774, 99
Kippenhahn R., Weigert A., 1967, Z. Astrophys., 65, 251
Kobayashi C., Tsujimoto T., Nomoto K., Hachisu I., Kato M., 1998, ApJ, 503, L155
Langer N., Deutschmann A., Wellstein S., H"oflich P., 2000, A&A, 362, 1046
Leibundgut B., 2000, A&AR, 10, 179
Lepo K., van Kerkwijk M., 2013a, ApJ, 771, 13
Lepo K., van Kerkwijk M., 2013b, in Di Stefano R., Orio M., Moe M., eds, Proc. IAU Symp. 281, Binary Paths to Type Ia Supernovae Explosions. Cambridge Univ. Press, Cambridge, 136
Li X. D., van den Heuvel E. P. J., 1997, A&A, 322, L9
Li W. D., Chornock R., Leaman J., Filippenko A. V., Poznanski D., Wang X., Ganeshalingam M., Mannucci F., 2011a, MNRAS, 412, 1473
Li W. D. et al., 2011b, Nature, 480, 348
Liu Z. W., Pakmor R., Röpke F. K., Edelmann P., Wang B., Kromer M., Hillebrandt W., Han Z. W., 2012, A&A, 548, A2
Liu Z. W., Pakmor R., Röpke F. K., Edelmann P., Hillebrandt W., Kerzendorf W. E., Wang B., Han Z. W., 2013, A&A, 554, A109
Livio M., Soker N., 1988, ApJ, 329, 764
Ma X., Chen X., Chen H., Denissenkov P. A., Han Z., 2013, ApJ, 778, L32
Maguire K. et al., 2013, MNRAS, 436, 222
Maoz D., Mannucci F., Nelemans G., 2014, ARA&A, 52, 107
Marietta E., Burrows A., Fryxell B., 2000, ApJS, 128, 615
Marion G. H. et al., 2016, ApJ, 820, 92
Mason E., 2011, A&A, 532, L11
Matteucci F., Greggio L., 1986, A&A, 154, 279
Mazeh T., Goldberg D., Duquennoy A., Mayor M., 1992, ApJ, 401, 265
Mazzali P. A., Benetti S., Stehle M., Branch D., Deng J., Maeda K., Nomoto K., Hamuy M., 2005a, MNRAS, 357, 200
Mazzali P. A. et al., 2005b, ApJ, 623, L37
Mazzali P. A. et al., 2014, MNRAS, 439, 1959

Downloaded from https://academic.oup.com/mnras/article-abstract/469/4/4763/3820926
by Said Business School user
on 16 February 2018

Meng X., Han Z., 2016, A&A, 588, A88
Meng X., Podsiadlowski Ph., 2013, ApJ, 778, L35
Meng X., Yang W., 2010a, ApJ, 710, 1310
Meng X., Yang W., 2010b, MNRAS, 401, 1118
Meng X., Yang W., 2011a, Sci. China Phys. Mech. Astron., 54, 2296
Meng X., Yang W., 2011b, RA&A, 11, 965
Meng X., Chen X., Han Z., 2007, PASJ, 59, 835
Meng X., Chen X., Han Z., 2008, A&A, 487, 625
Meng X., Chen X., Han Z., 2009a, MNRAS, 395, 2103
Meng X., Chen X., Han Z., Yang W., 2009b, RA&A, 9, 1259
Meng X., Yang W., Geng X., 2009c, PASJ, 61, 1251
Meng X., Yang W., Geng X., 2010, New Astron., 15, 343
Meng X., Gao Y., Han Z., 2015, Int. J. Mod. Phys. D, 24, 14
Mennickent R. E., Honeycut R. K., 1995, Inf. Bull. Var. Stars, 4232, 1
Meyer F., Meyer-Hofmeister E., 1979, A&A, 78, 167
Miller G. E., Scalo J. M., 1979, ApJS, 41, 513
Newsham G., Starrfield S., Timmes F., 2014, in Woudt A., Ribeiro V. A. R. M., eds, ASP Conf. Ser. Vol. 490, Stella Novae: Past and Future Decades. Astron. Soc. Pac., San Francisco, p. 287
Nielsen M., Dominik C., Nelemans G., Voss R., 2013, A&A, 549, A32
Nomoto K., 1982, ApJ, 253, 798
Nomoto K., Nariai K., Sugimoto D., 1979, PASJ, 31, 287
Nomoto K., Thielemann F.-K., Yokoi K., 1984, ApJ, 286, 644
Nomoto K., Umeda H., Hachisu I., Kato M., Kobayashi C., Tsujimoto T., 1999, in Truran J., Niemeyer T., eds, Type Ia Suppernova: Theory and Cosmology. Cambridge Univ. Press, New York, p. 63
Nomoto K., Uenishi T., Kobayashi C., Umeda H., Ohkubo T., Hachisu I., Kato M., 2003, in Hillebrandt W., Leibundgut B., eds, ESO/Springer serious 'ESO Astrophysics Symposia', From Twilight to Highlight: The Physics of supernova. Springer, Berlin-Verlag, p. 115
Nomoto K., Saio H., Kato M., Hachisu I., 2007, ApJ, 663, 1269
Paczyński B., 1976, in Eggleton P. P., Mitton S., Whelan J., eds, Structure and Evolution of Close Binaries. Kluwer, Dordrecht, p. 75
Pakmor R., Röopke F. K., Weiss A., Hillebrandt W., 2008, A&A, 489, 943
Pakull M. W., Moch C., Bianchi L., Thomas H. C., Guibert J., Beaulieu J. P., Grison P., Schaeidt S., 1993, A&A, 278, L39
Pan K., Ricker P. M., Taam R. E., 2012a, ApJ, 750, 151
Pan K., Ricker P. M., Taam R. E., 2012b, ApJ, 760, 21
Parthasarathy M., Branch D., Jeffery D. J., Baron E., 2007, NewAR, 51, 524
Patat F. et al., 2007, Science, 317, 924
Patat F. et al., 2013, A&A, 549, A62
Patnaude D. J., Badenes C., Park S., Laming J. M., 2012, ApJ, 756, 6
Perlmutter S. et al., 1999, ApJ, 517, 565
Piersanti L., Cassisi S., Iben I., Jr, Tornambé A., 2000, ApJ, 535, 932
Piro A. L., Chang P., 2008, ApJ, 678, 1158
Podsiadlowski Ph., 2003, preprint (astro-ph/0303660)
Podsiadlowski Ph., Joss P. C., Rappaport S., 1990, A&A, 227, L9
Podsiadlowski Ph., Rappaport S., Pfahl E. D., 2002, ApJ, 565, 1107
Pols O. R., Tout C. A., Eggleton P. P., Han Z., 1995, MNRAS, 274, 964
Pols O. R., Tout C. A., Schröder K. P., Eggleton P. P., Manners J., 1997, MNRAS, 289, 869
Pols O. R., Schröder K. P., Hurly J. R., Tout C. A., Eggleton P. P., 1998, MNRAS, 298, 525
Powell L. C., Slyz A., Devriendt J., 2011, MNRAS, 414, 3671
Prieto J. L., Stanek K. Z., Beacom J. F., 2008, ApJ, 673, 999
Reimers D., 1975, Mémoires of the Société Royale des Sciences de Liège, 8, 369
Riess A. et al., 1998, AJ, 116, 1009
Rodney S. A. et al., 2012, ApJ, 746, 5
Rodney S. A. et al., 2015, AJ, 150, 156
Ruiz-Lapuente P. et al., 2004, Nature, 431, 1069
Sahman D. I., Dhillon V. S., Marsh T. R., Moll S., Thoroughgood T. D., Watson C. A., Littlefair S. P., 2013, MNRAS, 433, 1588
Schaefer B. E., 1990, ApJ, 355, L39
Schaefer B. E., Ringwald F. A., 1995, ApJ, 447, L45
Schröder K. P., Cuntz M., 2007, A&A, 465, 593
Schröder K. P., Pols O. R., Eggleton P. P., 1997, MNRAS, 285, 696
Shappee B. J., Kochanek C. S., Stanek K. Z., 2013, ApJ, 765, 150
Shen K. J., Bildsten L., 2007, ApJ, 660, 1444
Simon J. D. et al., 2009, ApJ, 702, 1157
Soker N., 2013, IAUS, 281, 72
Sternberg A. et al., 2011, Science, 333, 856
Thoroughgood T. D., Dhillon V. S., Littlefair S. P., Marsh T. R., Smith D. A., 2001, MNRAS, 327, 1323
Timmes F. X., Diehl R., Hartmann D. H., 1997, ApJ, 479, 760
van den Bergh S., Tammann G. A., 1991, ARA&A, 29, 363
van den Heuvel E. P. J., Bhattacharya D., Nomoto K., Rappaport S. A., 1992, A&A, 262, 97
Wang B., Han Z., 2012, New Astron. Rev., 56, 122
Wang X., Li W., Filippenko A. V., Foley R. J. Smith N., Wang L., 2008, ApJ, 677, 1060
Wang B., Li X., Han Z., 2010, MNRAS, 401, 2729
Webbink R. F., 1984, ApJ, 277, 355
Webbink R. F., 1988, in Mikolajewska J., Friedjung M., Kenyon S. J., Viotti R., eds, The Symbiotic Phenomenon. Kluwer, Dordrecht, p. 311
Wheeler J. C., Pooley D., 2013, ApJ, 762, 75
Whelan J., Iben I., 1973, ApJ, 186, 1007
Willems B., Kolb U., 2004, A&A, 419, 1057
Williams B. J. et al., 2011, ApJ, 741, 96
Woosley S. E., Kasen D., 2011, ApJ, 734, 38
Wu T., Li Y., Hekker S., 2014, ApJ, 781, 44
Xue Z., Schaefer B. E., 2015, ApJ, 809, 183
Yang Y. et al., 2017, ApJ, 834, 60
Yoon S.-C., Langer N., 2004a, A&A, 419, 645
Yoon S.-C., Langer N., 2004b, A&A, 425, 217
Yungelson L., Livio M., Tutukou A., Kenyon S. J., 1995, ApJ, 447, 656

APPENDIX: THE METHOD FOR CALCULATING THE CE MASS IN OUR CODE

In Section 2.2, equations (7), (8), (10) and (11) form a coupled set of equations that determine the mass in the CE. Here, we show how this is determined in our code. The main idea is that the formation of the CE and the mass loss from the CE surface may be divided into two steps, i.e. the CE forms first, and then the wind begins to blow. In our code, there is a transition value $M_{\rm CE}^{'}$, which is determined by

$$M_{\rm CE,i+1}^{'} = M_{\rm CE,i} + (|\dot{M}_2|_{\rm i} - \dot{M}_{\rm WD,i}) \cdot \Delta t, \tag{A1}$$

where the initial value of $M_{\rm CE,\,0} = 0$. Then, putting the transition value into equation (10), we may get the CE radius. Based on equations (3), (5) and (6), the frictional luminosity $L_{\rm f}$ may be obtained, and then the total luminosity $L_{\rm tot} = L_{\rm nuc} + L_2 + L_{\rm f}$, where $L_{\rm nuc}$ is nuclear energy for stable hydrogen burning and L_2 is the secondary luminosity. $L_{\rm nuc}$ is obtained from equation (9). Therefore, according to equation (8), we may get the mass-loss rate $\dot{M}_{\rm wind}$, where the CE mass is also the transition value from equation (A1). The CE mass is then calculated according to

$$M_{\rm CE,i+1} = M_{\rm CE,i+1}^{'} - \dot{M}_{\rm wind,i} \cdot \Delta t. \tag{A2}$$

Equation (A1) + equation (A2) deduces to

$$\begin{aligned} M_{\rm CE,i+1} &= M_{\rm CE,i} + (|\dot{M}_2|_{\rm i} - \dot{M}_{\rm WD,i} - \dot{M}_{\rm wind,i}) \cdot \Delta t \\ &= M_{\rm CE,i} + \dot{M}_{\rm CE,i} \cdot \Delta t, \end{aligned} \tag{A3}$$

which is exactly the same as equation (11).

This paper has been typeset from a TEX/LATEX file prepared by the author.

Downloaded from https://academic.oup.com/mnras/article-abstract/469/4/4763/3820926
by Said Business School user
on 16 February 2018